# Winter-mixing preconditioning of the spring phytoplankton bloom in the Bay of Biscay

**Authors:** Ricardo González-Gil[1*], Fernando González Taboada[2,3], Carlos Cáceres[4], John L. Largier[5], Ricardo Anadón[1]

* Contact author e-mail: rgonzalezgil@gmail.com

1. Área de Ecología, Dpto. Biología de Organismos y Sistemas, Universidad de Oviedo, C/Valentín Andrés Álvarez s/n, E33071 Oviedo, Asturias, Spain.

2. Atmospheric and Oceanic Sciences, Princeton University, Princeton, NJ, USA.

3. Geophysical Fluid Dynamics Laboratory, National Oceanic and Atmospheric Administration, Princeton, NJ 08540 USA.

4. Dept. of Mathematics and Statistics, University of Strathclyde, 26 Richmond St, Glasgow G1 1XQ, UK

5. Bodega Marine Laboratory, University of California, Davis, 2099 Westside Drive, Bodega Bay, CA 94923-0247 USA.

**Running head:** Winter mixing and spring bloom

**Key words:** winter mixing, spring phytoplankton bloom, time series, global warming, remote sensing, Bay of Biscay

## Abstract

The spring phytoplankton bloom plays a key role in the dynamics of temperate and polar seas. Nevertheless, the mechanisms and processes behind these blooms remain a subject of considerable debate. We analyzed the influence of deep mixing during winter on the spring phytoplankton bloom in the Cantabrian Sea (southern Bay of Biscay). To this end, we combined long-term physical and biogeochemical in situ data (1993-2012) and satellite observations (1997-2012). Deeper winter mixing led to higher nitrate and chlorophyll concentrations through the water column during the spring bloom. However, this effect was modified by short-term variability in near-surface stratification in spring. Winter-mixing preconditioning also influenced different spring bloom metrics: deeper and later mixing in winter was followed by later blooms with a larger peak. In these enhanced blooms, nitrate was taken up at faster rates, indicating higher rates of phytoplankton production. Winters with weaker mixing (that led to weaker spring blooms) were associated with warmer surface temperatures. This relationship suggests that the multi-decadal trend towards warmer surface temperatures in the Bay of Biscay may promote a decrease in the magnitude of the spring bloom, which could impact upper trophic levels and also deep carbon export in the future.

## Introduction

Every year, the spring phytoplankton bloom reappears in temperate and polar seas, turning surface waters green. This phenomenon has fascinated researchers since the early days of oceanography in the 19th century (Banse 1992; Fischer et al. 2014). In the last decades, satellite images of surface chlorophyll concentration led to a renewed interest in phytoplankton blooms by revealing their ubiquity and large spatial extent (Parsons and Lalli 1988; Yoder et al. 1993; McClain 2009). Vernal phytoplankton blooms pump important amounts of atmospheric carbon into deep oceanic waters, making them a key component of biogeochemical cycles (Longhurst and Harrison 1989; Falkowski et al. 1998; Sarmiento and Gruber 2006). At the same time, these blooms support much of the annual productivity at higher trophic levels, including many exploited species (Hjort 1914; Cushing 1990; Townsend et al. 1994).

The North Atlantic spring phytoplankton bloom is the most pronounced bloom in open ocean waters (Yoder et al. 1993), although its characteristics vary substantially in space and time (Ueyama and Monger 2005; Racault et al. 2012; González Taboada and Anadón 2014). Interannual changes in the timing and magnitude of phytoplankton blooms can lead to a trophic match-mismatch that modulates the survival of upper trophic levels, including commercially fished stocks (Cushing 1990; Platt et al. 2003; Durant et al. 2007; Koeller et al. 2009; Kristiansen et al. 2011). With such important impacts, there is a growing interest in understanding the factors that promote interannual variability in the characteristics of the spring phytoplankton bloom, especially in the context of global climate change (Racault et al. 2012). Different hypotheses have been proposed to explain the mechanisms that trigger the onset of spring blooms, leading to an intense and ongoing debate (Behrenfeld and Boss 2014; Lindemann and St. John 2014; Chiswell et al. 2015;

Ferreira et al. 2015). Most of the drivers involved in these mechanisms also influence the magnitude of the bloom (Follows and Dutkiewicz 2002; Henson et al. 2006; Henson et al. 2009).

Among the physical processes that influence bloom development, deep mixing in winter stands out due to its crucial role in preconditioning the environment for a phytoplankton bloom in the next spring. During winter, deep convective mixing leads to the replenishment of near-surface nutrients (Williams and Follows 2003). Inorganic nitrogen compounds, such as nitrate, are often limiting for phytoplankton productivity (Falkowski et al. 1998; Moore et al. 2013) and thus, their availability is an important factor controlling the development of spring blooms (see for example Sambrotto et al. 1986; Sieracki et al. 1993; D'Ortenzio et al. 2014). As winter progresses towards spring, nutrients in surface layers become isolated from deeper waters with the onset of seasonal stratification. This sets an upper bound on the amount of nutrients available for phytoplankton in spring because, for many species, the access to nutrients below the seasonal thermocline is very limited. Deep mixing also constrains phytoplankton growth and the density of seeding populations by reducing the residence time of individual phytoplankters in the euphotic layer (Sverdrup 1953), although it simultaneously decreases encounter rates with grazers due to dilution effects (Yoshie et al. 2003; Behrenfeld 2010; Behrenfeld and Boss 2014).

With such a variety of effects operating together, the question that arises is: how and to what extent does winter mixing influence the spring phytoplankton bloom? Several studies have investigated the role of winter mixing in determining the magnitude of spring blooms (e.g. Follows and Dutkiewicz 2002; Henson et al. 2009; Martinez et al. 2011), but we are not aware of any analyses of how winter mixing affects other characteristics such

as bloom timing and duration. In addition, phytoplankton blooms are usually analyzed either in terms of changes in surface or in depth-integrated chlorophyll, ignoring potential changes in vertical structure (Chiswell et al. 2015). Indeed, phytoplankton community structure varies consistently across vertical gradients in the water column, with marked changes in physiological, ecological and taxonomic patterns (Reynolds 2006).

A proper characterization of spring phytoplankton blooms demands high frequency sampling to capture rapid changes in phytoplankton biomass (Rantajärvi et al. 1998). This imposes a major constraint on analyses of change in phytoplankton phenology. The availability of daily satellite ocean color measurements only partially alleviates this problem, given the lack of data during cloudy periods and the limitation of measurements to surface waters (McClain 2009). On the other hand, traditional approaches based on in situ sampling allow the collection of information at different depths, but sustained sampling based on recurrent oceanographic cruises spanning many years is limited to lower frequency sampling (Karl 2010; Church et al. 2013).

We combined monthly in situ data (1993-2012) with quasi-daily satellite observations (1997-2012) to analyze the influence of deep winter mixing on the spring phytoplankton bloom in the central Cantabrian Sea (southern Bay of Biscay). In this temperate sea, nutrient supply to upper layers is largely driven by deep mixing processes during winter (Llope et al. 2007; Hartman et al. 2013), leading to a well-developed spring bloom that is a major feature of the seasonal cycle of phytoplankton (Varela 1996). First, we examined the relationship of winter mixing with nitrate and phytoplankton concentrations through the water column during the spring bloom, considering also short-term variability in the stability of the upper layer. Next, we assessed how inter-annual changes in winter mixing modulate the timing, duration and intensity of the surface expression of the spring bloom.

Finally, we explored how changes in surface temperature impacts the development of the spring phytoplankton bloom through its influence on winter mixing. Through these analyses, we assess the relative importance of winter mixing on the interannual variability of the spring phytoplankton bloom in temperate seas.

## Material and methods

The central Cantabrian Sea (southern Bay of Biscay, Fig. 1) has been sampled intensively for the last two decades as part of the Spanish long-term monitoring network RADIALES (www.seriestemporales-ieo.com, Valdés et al. 2002; Valdés et al. 2007). Here, we used samples collected monthly between 1993 and 2012 at station E3, the most oceanic station of the Cudillero transect. Station E3 is located close to the shelf break, over the Avilés Canyon (06º10'W, 43º46'N, depth 870 m), and it reflects oceanic conditions typical of a temperate sea. A detailed description of the station and information about the protocols used can be found in Llope *et al.* (2006). We combined these in situ samples with daily satellite data for surface chlorophyll *a* concentration ([Chl *a*]$_{SAT}$) and sea surface temperature (SST) averaged over a 0.25º quadrangular pixel centered at 6.125ºW and 43.875ºN (Fig. 1).

### In situ oceanographic observations

We used 500-m CTD profiles (SeaBird-25) to assess the intensity of winter mixing between 1993 and 2012. We estimated mixed layer depth (hereafter $MLD_{0.5}$) as the depth where the temperature decreases 0.5ºC with respect to the temperature at 10 m depth (Monterey and Levitus 1997). Then, we determined annual maximum winter mixing depths ($WMD_{max}$) from $MLD_{0.5}$ estimates in winter months (January, February or March), before the spring [Chl *a*]$_{SAT}$ maximum (see *Statistical analysis and spring bloom metrics* section). Incomplete profiles or those showing a thermal inversion were rejected to avoid under- or over-estimating $MLD_{0.5}$, respectively. Thermal inversions were identified in profiles where temperatures exceeded the 10-m-depth temperature by 0.1°C or more over at least 25 m. It is important to note that, due to the monthly sampling frequency, the deep

mixing process leading to the measured $WMD_{max}$ could have occurred days or weeks before the monthly sampling date, or that later events could lead to deeper mixing before sampling the next profile.

Short-term changes in near-surface stratification can mask the influence of winter mixing on spring bloom characteristics. To control for this masking effect, we included the estimated depth of near-surface stratification in our analysis. We estimated the depth of the near-surface stratification (hereafter $MLD_{0.1}$) on each sampling date from the depth at which temperature is 0.1ºC lower than at 4 m depth (or at 6 m depth, if 4 m was missing; see Dever et al. 2006; Chiswell 2011; Houpert et al. 2015). Daily variations in the near-surface stratification depth affect phytoplankton vertical distribution and the local conditions experienced by phytoplankton cells during the spring bloom (Chiswell 2011; Chiswell et al. 2015; Franks 2015). Heating of surface water is the primary source of stratification, which suppresses near-surface turbulence (Franks 2015). Therefore, the depth of thermal stratification largely controls how far phytoplankton cells can be moved away from the surface and thus determines the amount of light received by phytoplankton.

We examined changes in observed nitrate and chlorophyll *a* (Chl *a*) concentrations in the upper 200 m to analyze the potential bottom-up effects of winter mixing on spring phytoplankton blooms. Nitrate is the most limiting nutrient of phytoplankton growth in the area (Llope et al. 2007), while Chl *a* data were used as a proxy for phytoplankton biomass. Both nitrate and Chl *a* samples were collected at eight depths (~ 0, 10, 20, 30, 40, 50, 75, 100, 150, 200 m) at station E3 using 5-L Niskin bottles. Nitrate samples were frozen and stored at -20ºC before measuring nitrate concentrations using a Technicon AAII Autoanalyser (Industrial Method 158-71 W/A) and a Skalar SANplus (Skalar Analytical B.V.). Post-cruise nitrate concentrations were converted from μmol $L^{-1}$ to

159 µmol $kg^{-1}$ using water density estimates at average laboratory conditions (22.5ºC and
160 98.6 kPa at 232 m.a.s.l.). Chl *a* concentrations were estimated by filtering samples
161 through GF-F filters (25 mm diameter), using 200 mL for low-Chl *a* samples, and 100
162 mL for high-Chl *a* samples. These filters were subsequently frozen at -20ºC. Then, Chl *a*
163 was extracted in 10 mL of 90% acetone over 24 h in darkness at 4ºC. Chl *a* concentrations
164 were measured using a Turner Designs 10 fluorometer following the method of Yentsch
165 and Menzel (1963).

166 We explored seasonal and interannual variability in Chl *a* and nitrate concentrations
167 through the water column using contour plots based on kriging interpolation (Nychka et
168 al. 2015). Before kriging, we used linear interpolation to ensure that the shape of vertical
169 profiles was locally preserved in the contour plots (i.e. by estimating concentrations every
170 two meters). We also used linear interpolation to estimate missing Chl *a* and nitrate
171 concentrations in the profile of a given date before calculating depth-integrated values.
172 Linear interpolation was preceded by a $\log_{10}$ transformation of Chl *a* concentrations. To
173 avoid unreliable estimates, we discarded profiles containing only one data point. We
174 calculated depth-integrated Chl *a* and nitrate using the trapezoidal rule. Depth-integrated
175 Chl *a* was calculated for ~0 to 200 m depth and regarded as a proxy of total phytoplankton
176 biomass in the water column. Nitrate was integrated from ~ 0 to 50 m depth, just below
177 the nitracline depth during the seasonal stratification (see Figs. 2 and 3). Nitrate in this
178 upper layer is extensively exploited by phytoplankton during the spring bloom. The
179 nitracline was defined by a threshold concentration of 1 µmol $kg^{-1}$, following Cullen and
180 Eppley (1981).

## Remote sensing data

We used a time series of remotely sensed surface Chl *a* concentration ([Chl *a*]$_{SAT}$) to characterize the development of the spring phytoplankton bloom. In temperate latitudes, [Chl *a*]$_{SAT}$ provides a reliable proxy of phytoplankton biomass (McClain 2009). Satellite retrievals were averaged over a 0.25 x 0.25º quadrangle covering station E3 (Fig. 1). Daily time series of [Chl *a*]$_{SAT}$ between September 1997 and December 2012 were retrieved from Level 3 (geolocated, corrected and averaged over a regular grid) SeaWiFS (Sept. 1997-Dec. 2007, reprocessing R2010.0) and Aqua MODIS (Jul. 2002-Dec. 2012, reprocessing R2013.1.1) standard mapped images (SMI) available at the Ocean Color Web (NASA OBPG 2015a; b). Estimates of [Chl *a*]$_{SAT}$ were derived using version six of the OC4 (SeaWiFS) and OC3M (Aqua MODIS) empirical band-ratio algorithms (O'Reilly et al. 2000, oceancolor.gsfc.nasa.gov/cms/atbd/chlor_a).

We also used remotely sensed sea surface temperature (SST, see *Statistical analysis and spring bloom metrics* section). The SST time series (from September 1981 to December 2012) was derived from the NOAA-Optimum Interpolation 1/4 Degree Daily Sea Surface Temperature Analysis (OISST version 2). The methods are described in Reynolds et al. (2007). The database of SST images is produced and maintained by C. Liu and R. W. Reynolds at NCDC (www.ncdc.noaa.gov/oisst). SST is one of the most important parameters in the dynamics of pelagic ecosystems: it has a direct effect on metabolic rates (Eppley 1972; Ikeda 1985), and it is an indicator of many physical processes that affect pelagic organisms, such as mixing and upwelling. Thus, we also explored the relationship between SST and the intensity of mixing in winter.

## Statistical analysis and spring bloom metrics

The characterization of the spring phytoplankton bloom and the influence of winter mixing differed depending on whether in situ data or remotely sensed data were used. In the case of in situ sampling, the availability of data through the entire water column allowed us to study variations in the development of the bloom at different depths, considering also concomitant changes in nitrate concentration. On the other hand, higher frequency satellite data allowed extraction of different bloom metrics, although this approach was restricted to surface waters. To conduct our analyses, we combined simple linear regressions and Generalized Additive Models (GAMs, Hastie and Tibshirani 1990). The main characteristic of GAMs is the inclusion of unspecified smooth functions to capture nonlinear relationships among the response and predictor variables (see *Supporting information* for further details). We assumed independent and identically distributed normal errors in all cases, which required $\log_{10}$ transformation of Chl *a* data before the analyses (both in situ and satellite). Model assumptions were checked by examining the distribution of residuals. All the statistical analyses were performed in R version 3.3.3 (R Core Team 2017) using RStudio interface version 1.0.143 (RStudio Team 2016). GAMs were fitted using the functions gam and t2 from the package mgcv (v1.8-17, Wood 2006; Wood et al. 2013). We also used the package LatticeKrig v6.2 (Nychka et al. 2016) for kriging interpolation. Figures were created using package ggplot2 (v2.2.1, Wickham 2009) and graphically improved in Inkscape (www.inkscape.org).

## Characterization of seasonality

We characterized the shape of the seasonal cycle for physical variables (SST, $MLD_{0.5}$ and $MLD_{0.1}$), nitrate and Chl *a*. We fitted the following GAM to each physical variable, depth-integrated nitrate and Chl *a*, surface nitrate concentration and $[\text{Chl } a]_{SAT}$ (all of them represented below as $y$):

$$y = a + f(t) + \varepsilon \quad (1)$$

The model includes an intercept ($a$), a 1D smooth function ($f$) to represent the seasonal curve as a function of day of the year ($t$) and an error term represented by $\varepsilon$ (see *Supporting information* for further specifications).

In the case of in situ Chl *a* and nitrate concentration, we estimated the seasonality through the water column using a GAM that included an interaction term between the day of the year ($t$) and depth ($z$):

$$y = a + te(t, z) + \varepsilon \quad (2)$$

where the interaction term $te(t, z)$ is a 2D smooth function (specifically, a tensor product) that captures the seasonal cycle of the vertical profiles of Chl *a* and nitrate concentration over the day of the year (Wood 2006).

## Analysis of the winter mixing effect based on in situ data

We first inspected the effect of deep mixing on depth-integrated nitrate in winter using a simple linear regression. Then, to examine the influence of winter mixing on spring-

bloom Chl *a* and nitrate concentrations through the water column, we identified the month with maximum surface Chl *a* concentration during the first half of each year. We considered this month as representative of conditions during the spring bloom. We formulated then a set of alternative models to explore the influence of $WMD_{max}$ and $MLD_{0.1}$ on vertical profiles of Chl *a* and nitrate that month (see Table 1). Alternative models were later compared based on Akaike Information Criterion (AIC, Burnham and Anderson 2002). The basic null model, which only included an intercept, was expanded by adding terms for the influence of depth and for the interaction effect between depth and either $WMD_{max}$ or $MLD_{0.1}$ (note that $WMD_{max}$ and $MLD_{0.1}$ were uncorrelated, $r$ = 0.11, p-value = 0.688). These interaction terms were included to capture a distinct depth-dependent effect of $WMD_{max}$ or $MLD_{0.1}$. We completed the analysis by testing the existence of an interaction effect between $WMD_{max}$ and $MLD_{0.1}$, although we limited this analysis to surface waters (See Table 2 for the list of models tested). This enabled an easier comparison with satellite information. Additionally, we explored this interaction effect for depth-integrated Chl *a*.

We concluded the analysis of profile data by examining the impact of winter mixing on new primary production ($PP_{new}$) during the spring bloom. Assuming that the effect of transport and external sources is negligible, we can ascribe the drawdown of nitrate in the upper layers mainly to phytoplankton uptake. This provides a rough approximation of $PP_{new}$ (mg C $m^{-2}$ $day^{-1}$) during the bloom:

$$PP_{new} \sim r_{C:N} \int_{50}^{0} \frac{1}{\Delta t} \left( [\mathrm{NO_3}]_{z,t_i} - [\mathrm{NO_3}]_{z,t_f} \right) \mathrm{d}z \qquad (3)$$

where the decay in nitrate concentration $[NO_3]$ at depth $z$ (mol $m^{-3}$) between February ($t_i$) and April ($t_f$) was integrated over the upper 50 m of the water column (i.e. from just below the nitracline depth during the seasonal stratification, see Figs. 2 and 3). For each season, we subtracted nitrate concentrations in February from those recorded in April to cover the entire bloom development. Differences in $[NO_3]$ were averaged over time using the difference in days between sampling dates, $\Delta t$. The factor used in the conversion from nitrate to carbon units ($r_{C:N} = 6.6$) was based on a constant C:N ratio averaged from the C:N ratios for the new production estimated by Körtzinger et al. (2001) in bloom and early bloom sampling stations during a meridional transect carried out in the Northeast Atlantic. This $r_{C:N}$ coincides with the ratio described by Redfield (1958) for the particulate organic matter in the ocean. We calculated $PP_{new}$ for each season and compared it with the intensity of winter mixing using a simple linear regression on $WMD_{max}$ measured during the preceding winter. We presumed that a positive relationship between $PP_{new}$ and $WMD_{max}$ would be indicative of the preconditioning effect of winter mixing on the spring bloom development.

## Spring bloom characterization based on satellite data

The high temporal resolution of $[\text{Chl } a]_{SAT}$ data allowed us to extend the analysis of interannual variability in the spring bloom. To do that, we fitted a GAM featuring a changing seasonal cycle among years both to $[\text{Chl } a]_{SAT}$ and SST data ($y$):

$$y = a + f(t|year) + \varepsilon \quad (4)$$

where $a$ corresponds to the intercept, $t$ to the day of the year, and $\varepsilon$ is an error term. The $f(t|year)$ term is included to capture changes in the seasonality among years. In the

model, the seasonal cycle starts in July 15$^{th}$ (or 14$^{th}$ in a leap year). This choice ensured that the seasonal term included the annual SST maximum and the SST minimum in the next year, both required to derive spring bloom metrics (see below). For [Chl *a*]$_{SAT}$, analyses conducted beforehand indicated that there is no need to account for differences in mean concentration or in the shape of the seasonal cycle between sensors (SeaWiFS and Aqua MODIS). Lack of [Chl *a*]$_{SAT}$ information during the period 1997-1998 resulted in unreliable estimates of bloom metrics that were not included in the main analyses.

We retrieved a series of metrics to characterize interannual changes in the spring bloom based on modelled time series of [Chl *a*]$_{SAT}$ (Eq. 4). We determined first the timing of the autumn bloom, which follows the annual SST maximum. The autumn bloom was defined as the first local maximum in [Chl *a*]$_{SAT}$ reached after at least 30 consecutive days of increase in [Chl *a*]$_{SAT}$ (this condition prevents confounding this bloom with a small rise in [Chl *a*]$_{SAT}$). Then, we defined spring *bloom rise* as the day when the seasonal curve of [Chl *a*]$_{SAT}$ increased at the fastest rate following the autumn bloom. If no autumn bloom was observed (i.e. only one [Chl *a*]$_{SAT}$ maximum occurred), then spring *bloom rise* was defined as the date when the [Chl *a*]$_{SAT}$ seasonal curve increased at the fastest rate. This criterion to identify the timing of the spring bloom avoids the use of an a priori chlorophyll threshold (for references discussing different criteria, see Brody et al. 2013; Blondeau-Patissier et al. 2014; González Taboada and Anadón 2014). We defined *bloom decay* as the day when the [Chl *a*]$_{SAT}$ seasonal curve decreased at the fastest rate after both the spring bloom maximum (i.e. the magnitude of the spring bloom peak, *max Chl a*) and minimum SST. The latter condition allows identification of the real spring bloom decay, avoiding confusion with an early, temporary decrease in [Chl *a*]$_{SAT}$ after reaching the *max Chl a*. The day of occurrence of the *max Chl a* was another timing metric (*max*

306 *Chl a day*). Finally, we identified the *bloom span* as the number of days between *bloom*
307 *rise* and *bloom decay*.

308 Once we calculated these bloom metrics for each year, we inspected the influence of
309 winter mixing on them by using linear regression analysis. We also used linear
310 regressions to analyze SST long-term trends and to explore the impact of SST on the
311 magnitude of winter mixing at different lags.

312

## Results

### Seasonality

Physical variables (SST, $MLD_{0.5}$, $MLD_{0.1}$) and both nitrate and Chl *a* concentrations at different depths, or integrated through the water column, all showed a clear seasonal pattern (Figs. 2 and 3). The seasonal cycle in SST exhibited a maximum of 20.34ºC in August and a minimum of 12.54ºC in March (Fig. 3a). In mid-winter (January and February), both $MLD_{0.5}$ and $MLD_{0.1}$ were deep, indicating a well-mixed water column (Fig. 3b). Some profiles showed shallower $MLD_{0.1}$ than $MLD_{0.5}$ during the well-mixed period, indicating that transient shallow and weak stratification may develop in winter, accounting for a shallow $MLD_{0.1}$ being observed above a deeper $MLD_{0.5}$ that may have formed days or even weeks before the sampling dates. As a consequence of the mixing, nitrate was homogeneously distributed through the water column in mid-winter (average concentration of 4.68 μmol $kg^{-1}$, Fig. 3c), which accounts for the annual maximum in the uppermost 50 m (Figs. 3c, 3e and 3g). At the end of February, a surface stratified layer started to form (shoaling of $MLD_{0.1}$), which is the beginning of seasonal stratification (Fig. 3b). Concurrently, surface nitrate started to decrease and was very low during the stratification period, from May to October (mean concentration in the top 20 m of 0.28 μmol $kg^{-1}$). This caused the formation of a marked nitracline at ~ 40 m depth (Figs. 2a and 3c).

In contrast to nitrate, Chl *a* exhibited higher concentrations in near-surface waters except in mid-winter, when mixing homogenized the water column, and in mid-summer when the chlorophyll maximum was observed close to the depth of the nitracline (Fig. 3d). Depth-integrated Chl *a* increased markedly in late December (Fig. 3f), although

surface concentrations only increased in late February with the onset of stratification (Figs. 3d and 3h). This fast increase in Chl *a* corresponds to the spring bloom and accounts for most of the seasonal depletion of near-surface nitrate. It represents the annual maximum in phytoplankton biomass, which generally occurred in March near-surface (Figs. 3d, 3h and 4) and ranged from 0.23 to 5.41 mg $m^{-3}$ (average Chl *a* concentration in the uppermost 20 m). The annual maximum decreased in magnitude with depth and occurred later at intermediate-depth waters from 30 to 50 m (Fig. 4). From June to September, Chl *a* concentrations remained low near-surface (Figs. 3d and 3h) with the maximum observed between 20 and 50 m (0.33 mg $m^{-3}$ on average). Surface Chl *a* concentration increased again during the autumn bloom, which usually peaked in November (Fig. 3d and 3h) and was weaker than the spring bloom (average Chl *a* concentration of 0.18-2.64 mg $m^{-3}$ in the uppermost 20 m).

## Effect of $WMD_{max}$ on the vertical structure of the spring bloom

Maximum winter mixing depths ($WMD_{max}$) exhibited inter-annual variability in both magnitude and timing (Fig. 5a). This variability affected the nutrient supply to surface layers: the deeper the $WMD_{max}$, the larger the depth-integrated nitrate over the upper 50 m (Figs. 5b and 5c). Winter mixing also affected nitrate levels and Chl *a* in spring blooms, as seen in Table 1. Data for March were used to analyze this effect, the month in which the near-surface spring bloom typically peaks (Figs. 3d, 3h and 4). The model that includes $WMD_{max}$ and $MLD_{0.1}$ as predictors of nitrate and Chl *a* concentrations performed best (Table 1). This indicates that both the past and recent history of water-column stratification (i.e. $WMD_{max}$ and $MLD_{0.1}$, respectively) have an effect on nitrate and Chl *a* concentrations during the spring bloom. This model shows that higher nitrate and Chl *a* concentrations in March follow winters with deeper $WMD_{max}$ (left panels in Fig. 6). The

positive effect of $WMD_{max}$ on nitrate concentration was more important towards the surface (i.e., the increase in the effect along the x axis is gradually larger towards shallower depths in the left panel of Fig. 6a). A similar effect was found for Chl *a*; the positive effect of $WMD_{max}$ was also strongest in surface waters and it became weaker at deeper depths, especially at intermediate layers (left panel in Fig. 6b). In both cases, the near-surface seasonal depletion of nutrients during stratification (Figs. 3c, 3e and 3g) can explain the higher near-surface sensitivity of nitrate and Chl *a* to winter mixing.

Contrary to the effect of $WMD_{max}$, the relationship between near-surface stratification depth ($MLD_{0.1}$) and either nitrate or Chl *a* concentrations in March varied markedly across depth (right panels in Fig. 6). In the case of nitrate, near-surface concentrations decrease when $MLD_{0.1}$ is shallow ($MLD_{0.1}$ ~ 0 to 75 m, right panel of Fig. 6a), with strongest decreases for shallowest $MLD_{0.1}$. This effect of $MLD_{0.1}$ on nitrate is consistent with rapid nutrient drawdown when phytoplankton blooms are confined within a thin surface layer (depth given by $MLD_{0.1}$). Consistent with this forcing, large Chl *a* concentrations are seen near-surface and at depth (below ~ 150 m) when $MLD_{0.1}$ is less than ~100 m (see right panel of Fig. 6b). The effect in other sections of the water column (below ~ 50 m for nitrate, but ~ 30-150 m for Chl *a*) peaked at intermediate $MLD_{0.1}$ (~ 50-125 m).

Table 2 summarizes the effect of $WMD_{max}$ and $MLD_{0.1}$ on surface nitrate and Chl *a* concentrations in March. In the case of nitrate, the model including only $MLD_{0.1}$ explained around three times more variability than the $WMD_{max}$ alone (Table 2); the model including an interaction showed a positive effect of $MLD_{0.1}$, which was similar along the entire $WMD_{max}$ range, and a decreasing positive effect of $WMD_{max}$ towards deeper $MLD_{0.1}$ (Fig. 7a). In the case of Chl *a*, the interaction model outcompeted the others (Table 2). For the analysis of the model outputs portrayed in Fig. 7b, we focused

on those regions of the sample space with observations. Surface Chl *a* concentration was maximum for deep $WMD_{max}$ and shallow $MLD_{0.1}$ and showed a secondary maximum for $MLD_{0.1}$ ~ 50-100 m. Depth-integrated Chl *a* in March, which was highly correlated with Chl *a* at 20-30 m depth (*Supporting information* Fig. S1a), showed a similar response pattern as surface Chl *a*. However, maximum depth-integrated Chl *a* showed approximately the same values for $MLD_{0.1}$ ~ 50-150 m as for deep $WMD_{max}$ and shallow $MLD_{0.1}$ (Fig. S1b).

The new primary production ($PP_{new}$) during the spring bloom, estimated from depth-integrated nitrate (0-50 m) depletion, was between 30 and 490 mg C $m^{-2}$ $day^{-1}$ (Fig. 8). We found a clear relationship between primary production and $WMD_{max}$ ($R^2$ = 0.41, p-value = 0.026). This model predicts an increase in $PP_{new}$ of ~ 64 mg C $m^{-2}$ $day^{-1}$ for every 100 m increase in $WMD_{max}$.

### Effect of $WMD_{max}$ on spring bloom metrics

High-resolution satellite data allowed characterization of the development of the spring phytoplankton bloom at the surface. Spring bloom phenology exhibited high interannual variability (Fig. 9), typically lasting ~ 90 days and peaking between February 17th and May 22nd (with mean date of April 4th). The magnitude of the bloom also varied between years, with [Chl *a*]$_{SAT}$ peak concentrations ranging from 0.53 to 1.43 mg m$^{-3}$. Changes in bloom magnitude were positively associated with $WMD_{max}$ (Fig. 10e), consistent with the analysis of in situ data. Later blooms with a shorter span followed winters with deeper mixing layers (Figs. 10a and 10i), although the effect of $WMD_{max}$ on these timing metrics remained more elusive ($R^2$ = 0.15, p-value = 0.165 for bloom rise; $R^2$ = 0.18, p-value = 0.133 for bloom span). As mentioned above, the bloom was more productive in years with deep $WMD_{max}$ (Fig. 8). Additionally, the later the $WMD_{max}$ occurred, the later the spring bloom peaked (Fig. 10h). A simple linear correlation analysis showed that $WMD_{max}$ and the $WMD_{max}$ sampling day were uncorrelated ($r$ = 0.30, p-value = 0.302).

### Impact of SST on $WMD_{max}$

The $WMD_{max}$ was negatively correlated with the SST, indicating that shallower $WMD_{max}$ follow warmer SST (Fig. 11a). These negative relationships were stronger for SST within ~ 60 days prior to the winter mixing event. Thus the December-March SST is most important in accounting for $WMD_{max}$, which mostly occurred in February and March (Fig. 5a). On the other hand, the SST seasonal cycle exhibited large interannual variation (Fig. 9). Beyond the observed linear trend (0.30 ºC decade$^{-1}$, 1981-2012), this variation reflects different rates of warming through the year, with largest values observed

during the period of seasonal stratification (spring to early autumn), when the trend frequently exceeds 0.30 ºC decade$^{-1}$ (Fig. 11b). This positive trend in SST indicates a long-term decline in $WMD_{max}$ and consequently in the magnitude of the spring bloom (see Fig. 10e). However, the short length of the record prevented a direct assessment of these trends and further exploration of this link is required.

## Discussion

Our results demonstrate a strong winter-mixing preconditioning of the development and characteristics of the spring phytoplankton bloom, modulated by near-surface stratification. Deeper and later winter mixing leads to more intense and later spring blooms. These more intense blooms are also more productive, as indicated by the faster nitrate decrease in near-surface waters. Additionally, we found that higher winter SST is associated with weaker mixing in winter, and thus also associated with weaker spring phytoplankton blooms.

The dynamics of the spring phytoplankton bloom remain a subject of active debate among marine scientists (see Behrenfeld and Boss 2014; Chiswell et al. 2015 for recent reviews). Some of this controversy arises from the adoption of different methods to characterize phytoplankton blooms (Ji et al. 2010), with contrasting findings depending on whether the analyses focused on surface or depth-integrated phytoplankton biomass (Chiswell et al. 2015). Nevertheless, both approaches disregard the depth-dependence of the phytoplankton response, which we describe here and that accounts for observed differences in timing and magnitude of the spring bloom.

The spring bloom exhibits yearly an apparent northward and southward progression in the Northern and Southern Hemisphere, respectively (Siegel et al. 2002; Henson et al. 2009; Chiswell et al. 2013). Analogously, in the Bay of Biscay and presumably also in other temperate regions (see for example Chiswell 2011), the spring bloom exhibits an apparent progression into subsurface layers as spring progresses and the water column stratifies. For upper layers, we understand this in terms of changes in the optimal nutrient and light conditions for phytoplankton growth (Klausmeier and Litchman 2001). In deep

447 layers, the seasonal timing of maximum Chl *a* might reflect a larger arrival of
448 phytoplankton cells from near-surface waters and positive phytoplankton growth during
449 winter, potentially due to a dilution effect on grazing (Behrenfeld 2010; Behrenfeld 2014;
450 Behrenfeld and Boss 2014). The observed seasonal increase in depth-integrated
451 phytoplankton biomass during winter supports this last aspect to some extent, but our
452 confidence is constrained by limited data availability during winter.

453 The observed seasonal cycle of Chl *a* in the Bay of Biscay shows that the development
454 of the spring bloom in surface waters occurs in March. A shift from a deep-mixing regime
455 (primarily buoyancy-driven) to a low-turbulence regime (mainly wind-driven) occurs
456 during this critical period (Huisman et al. 1999; Chiswell et al. 2013; Brody and Lozier
457 2014; 2015; Chiswell et al. 2015). This period coincides also with the onset of the
458 seasonal thermal stratification, triggered by a change to positive air-sea heat fluxes
459 (Chiswell 2011; Taylor and Ferrari 2011; Ferrari et al. 2015). Nitrate concentration at the
460 beginning of the spring bloom is largely controlled by the magnitude of deep mixing
461 events in the prior winter, as already shown by Hartman et al. (2013). However, inter-
462 annual changes in the characteristics of upper water masses and different hydrographic
463 processes (e.g. the Iberian Poleward Current, IPC) can modulate the effect of winter
464 mixing on nutrient preconditioning (Llope et al. 2007).

465 Winter convective mixing increases near-surface nutrient concentration directly
466 through nutrient entrainment from deep waters (Mann and Lazier 2006; Sarmiento and
467 Gruber 2006). Additionally, it reduces the time spent by phytoplankton in the euphotic
468 layer, lowering population growth rates (Sverdrup 1953), and also diluting phytoplankton
469 concentrations (Evans and Parslow 1985; Backhaus et al. 2003; D'Asaro 2008). Both
470 processes reduce nutrient uptake by phytoplankton in the upper ocean. However, this

dilution through mixing also reduces encounter rates with potential grazers, lowering the grazing pressure on phytoplankton population in winter (Yoshie et al. 2003; Behrenfeld 2010; Behrenfeld and Boss 2014). Combining the arguments presented above, deeper winter mixing can lead to a high-nutrient, low-grazing environment that may positively precondition phytoplankton growth during the spring bloom. Indeed, our analysis demonstrates that deeper winter mixing is associated with higher nutrient concentrations and more intense blooms in the southern Bay of Biscay.

The physical structure of the water column during the spring bloom, characterized by near-surface stratification, plays also an important role in shaping the vertical distribution of phytoplankton (Chiswell 2011; Brody and Lozier 2015). The thickness of the stratified layer determines how far phytoplankton can be moved downward, away from maximum light intensities (Franks 2015). Shoaling stratification in March keeps phytoplankton closer to the surface and exposed to higher aggregate light, leading to an increase in their growth rates (Chiswell 2011), and rapid removal of nitrate from these surface waters. We observed that surface phytoplankton biomass was enhanced by shallow-intermediate stratified layers, especially after a favorable preconditioning by mid-large winter mixing events. Higher Chl *a* concentrations at depth during shallow-intermediate stratification and after mid-large winter mixing may be due to larger fluxes of sinking cells due to enhanced phytoplankton growth in the upper layers (Falkowski et al. 1998; Sanders et al. 2014). In temperate seas such as the Bay of Biscay, diatoms become the dominant phytoplankton group during the spring bloom (Fernández and Bode 1994) and their sinking rates can be greater than 100 m $d^{-1}$, enhanced by particle aggregation (Smayda 1970; Lampitt 1985; Smetacek 1985; Burd and Jackson 2009). Thus, increased diatom growth in the surface during the bloom might lead to a rapid export of phytoplankton to

waters several hundreds of meters below. In our study area, this hypothesis is supported by the large pulses of biogenic silica collected by deep sediment traps during the spring blooms of 2012 and 2013 (Rumín-Caparrós et al. 2016; traps were moored at 1178 and 1154 m depth over the Avilés Canyon and westwards over the open slope, respectively).

Winter-mixing preconditioning also affected different metrics of the spring bloom in the surface layer. As observed in March for in situ Chl *a* concentrations, the high nutrient environment caused by deeper winter mixing events was associated with larger spring bloom peaks. This positive effect of deep convective mixing on the spring bloom has been observed in other areas of the North Atlantic (Martinez et al. 2011; Behrenfeld et al. 2013). However, our results demonstrate that enhanced nitrate concentrations following strong winter mixing also lead to a more rapid uptake of nutrients in spring. This rapid consumption reflects a larger accumulation of phytoplankton biomass and results in a shorter but more intense bloom. In this way, deeper mixing leads to higher community productivity in the Bay of Biscay (Hartman et al. 2013) and larger peaks in spring zooplankton biomass and abundance (González-Gil et al. 2015). This bottom-up perspective is also compatible with top-down mechanisms raised in the context of the Dilution-Recoupling Hypothesis (Behrenfeld 2010). The release of phytoplankton from grazing pressure in winters with enhanced mixing could entail the development of a larger seeding population and a bloom of a greater magnitude. Interestingly, a lower grazing rate could also reduce in situ nutrient regeneration and foster nutrient consumption by enabling higher accumulations of phytoplankton biomass (Banse 1992), with the overall result of more intense blooms with a shortened span.

Strong surface cooling processes due to heat losses are one of the major drivers of deep convective events in winter, as observed in 2005 in the Bay of Biscay (Somavilla et al.

519 2009; Acuña et al. 2010; Somavilla Cabrillo et al. 2011). Also, intense winds related to
520 winter storms may contribute to stirring of the water column during deep mixing (Henson
521 et al. 2006). If any or both of these processes occur at the end of winter, they could delay
522 the beginning of thermal stratification or break it temporarily during its initial phase.
523 Thermal stratification of the water column is required for full development of the near-
524 surface spring bloom (Chiswell 2011; Chiswell et al. 2015). Thus, later deep mixing
525 events associated with lower atmospheric temperatures and gales at the end of winter
526 would delay the spring bloom climax (Townsend et al. 1994; Henson et al. 2006; Álvarez
527 et al. 2009). This could explain our observation that later deep winter mixing events
528 caused later spring bloom peaks.

529 The trend towards surface warming in the southern Bay of Biscay in winter is
530 consistent with both observational and model-based increases in heat content in North
531 Atlantic surface waters (Danabasoglu et al. 2012; Taboada and Anadón 2012). A larger
532 increase in surface heat content relative to deeper layers represents increasing stability
533 and the need for larger energy inputs to mix the water column (Levitus et al. 2012). The
534 presumed decay in winter mixing associated with warming surface waters can be
535 expected to cause a decline in the magnitude of the spring phytoplankton bloom in the
536 Cantabrian Sea. Less intense blooms would decrease the strength of the biological pump
537 (Falkowski et al. 1998; Sanders et al. 2014), and they can also lead to a trophic mismatch
538 and a decrease in the production of upper trophic levels (Durant et al. 2007). Nevertheless,
539 the short length of the series analyzed in this study recommends caution in interpreting
540 trend results (e.g. Henson et al. 2010).

541 The impact of large-scale climate patterns such as the North Atlantic Oscillation
542 (NAO, Hurrell and Deser 2009) deters a simple interpretation of the long-term variability

in the Bay of Biscay associated with climate change. Indeed, changes in the intensity of winter mixing have been linked to changes in atmospheric circulation and air-sea heat fluxes in the Bay of Biscay associated with alternating phases of the NAO (Somavilla Cabrillo et al. 2011). Positive NAO promotes surface warming and shallower mixing in winter. However, extremely deep winter mixing events were common following a decade-long switch in NAO state starting in the mid-1990s. These strong winter mixing events are also associated with negative anomalies of the East Atlantic (EA) pattern that bring cold, northerly winds into the southern Bay of Biscay (Somavilla et al. 2009). Although continued warming might eventually conceal these effects, the consequences of changes in winter mixing, spring stratification and the interaction with long-term forcing remains elusive. Together, our findings recommend a continued monitoring and further analysis of potential changes in plankton phenology in the Bay of Biscay.

## Conclusions

Deep winter-mixing preconditioning affects nitrate and Chl *a* concentrations during the spring phytoplankton bloom in oceanic waters of the southern Bay of Biscay. Deeper winter mixing enhances phytoplankton biomass and nitrate concentrations during spring through the entire water column. On shorter time scales, the physical structure of the water column, characterized by the depth of the surface stratified layer, had an important role in shaping the vertical profiles of nitrate and phytoplankton. Our results show that deeper and later winter mixing events led to later and more intense spring blooms. The faster rate of nitrate uptake during this type of bloom indicates enhanced primary production. Finally, we found that warm surface temperatures, especially in winter, were associated with weaker mixing of the water column and consequently, with a smaller spring bloom peak. Observations and predictions of increasing surface temperature in winter thus suggest a potential weakening of the spring bloom and a reduction of upper trophic productivity and deep carbon export in the Bay of Biscay. This might also be observed in other temperate areas in the future.

## References


Acuña, J. L., M. López-Alvarez, E. Nogueira, and F. González-Taboada. 2010. Diatom flotation at the onset of the spring phytoplankton bloom: an *in situ* experiment. Mar. Ecol. Prog. Ser. **400:** 115-125. doi:10.3354/meps08405

Álvarez, E., E. Nogueira, J. L. Acuña, M. López-Álvarez, and J. A. Sostres. 2009. Short-term dynamics of late-winter phytoplankton blooms in a temperate ecosystem (Central Cantabrian Sea, Southern Bay of Biscay). J. Plankton Res. **31:** 601-617. doi:10.1093/plankt/fbp012

Backhaus, J. O., E. N. Hegseth, H. Wehde, X. Irigoien, K. Hatten, and K. Logemann. 2003. Convection and primary production in winter. Mar. Ecol. Prog. Ser. **251:** 1-14. doi:10.3354/meps251001

Banse, K. 1992. Grazing, temporal changes of phytoplankton concentrations, and the microbial loop in the open sea, p. 409-440. *In* P. G. Falkowski and A. D. Woodhead [eds.], Primary productivity and biogeochemical cycles in the sea. Plenum Press.

Behrenfeld, M. J. 2010. Abandoning Sverdrup's critical depth hypothesis on phytoplankton blooms. Ecology **91:** 977-989. doi:10.1890/09-1207.1

Behrenfeld, M. J. 2014. Climate-mediated dance of the plankton. Nat. Clim. Change **4:** 880-887. doi:10.1038/nclimate2349

Behrenfeld, M. J., and E. S. Boss. 2014. Resurrecting the ecological underpinnings of ocean plankton blooms. Annu. Rev. Mar. Sci. **6:** 167-194. doi:10.1146/annurev-marine-052913-021325

Behrenfeld, M. J., S. C. Doney, I. Lima, E. S. Boss, and D. A. Siegel. 2013. Annual cycles of ecological disturbance and recovery underlying the subarctic Atlantic spring plankton bloom. Glob. Biogeochem. Cycles **27:** 526-540. doi:10.1002/gbc.20050

Blondeau-Patissier, D., J. F. R. Gower, A. G. Dekker, S. R. Phinn, and V. E. Brando. 2014. A review of ocean color remote sensing methods and statistical techniques for the detection, mapping and analysis of phytoplankton blooms in coastal and open oceans. Prog. Oceanogr. **123:** 123-144. doi:10.1016/j.pocean.2013.12.008

Brody, S. R., and M. S. Lozier. 2014. Changes in dominant mixing length scales as a driver of subpolar phytoplankton bloom initiation in the North Atlantic. Geophys. Res. Lett. **41:** 3197-3203. doi:10.1002/2014GL059707

Brody, S. R., and M. S. Lozier. 2015. Characterizing upper-ocean mixing and its effect on the spring phytoplankton bloom with in situ data. ICES J. Mar. Sci. **72:** 1961-1970. doi:10.1093/icesjms/fsv006

Brody, S. R., M. S. Lozier, and J. P. Dunne. 2013. A comparison of methods to determine phytoplankton bloom initiation. J. Geophys. Res.: Oceans **118:** 2345-2357. doi:10.1002/jgrc.20167

Burd, A. B., and G. A. Jackson. 2009. Particle aggregation. Annu. Rev. Mar. Sci. **1:** 65-90. doi:10.1146/annurev.marine.010908.163904

Burnham, K. P., and D. R. Anderson. 2002. Model selection and multimodel inference: a practical information-theoretic approach. Springer-Verlag.

Cullen, J., and R. Eppley. 1981. Chlorophyll maximum layers of the Southern California Bight and possible mechanisms of their formation and maintenance. Oceanol. Acta **4:** 23-32. http://archimer.ifremer.fr/doc/00121/23207/.

Cushing, D. 1990. Plankton production and year-class strength in fish populations: an update of the match/mismatch hypothesis. Adv. Mar. Biol. **26:** 249-293. doi:10.1016/S0065-2881(08)60202-3

Chiswell, S. M. 2011. Annual cycles and spring blooms in phytoplankton: don't abandon Sverdrup completely. Mar. Ecol. Prog. Ser. **443:** 39-50. doi:10.3354/meps09453

Chiswell, S. M., J. Bradford-Grieve, M. G. Hadfield, and S. C. Kennan. 2013. Climatology of surface chlorophyll a, autumn-winter and spring blooms in the southwest Pacific Ocean. J. Geophys. Res.: Oceans **118:** 1003-1018. doi:10.1002/jgrc.20088

Chiswell, S. M., P. H. R. Calil, and P. W. Boyd. 2015. Spring blooms and annual cycles of phytoplankton: a unified perspective. J. Plankton Res. **37:** 500-508. doi:10.1093/plankt/fbv021

Church, M. J., M. W. Lomas, and F. Muller-Karger. 2013. Sea change: Charting the course for biogeochemical ocean time-series research in a new millennium. Deep Sea Res. Part II **93:** 2-15. doi:10.1016/j.dsr2.2013.01.035

D'Asaro, E. A. 2008. Convection and the seeding of the North Atlantic bloom. J. Mar. Syst. **69:** 233-237. doi:10.1016/j.jmarsys.2005.08.005

D'Ortenzio, F. and others. 2014. Observing mixed layer depth, nitrate and chlorophyll concentrations in the northwestern Mediterranean: A combined satellite and NO3 profiling floats experiment. Geophys. Res. Lett. **41:** 6443-6451. doi:10.1002/2014GL061020

Danabasoglu, G., S. C. Bates, B. P. Briegleb, S. R. Jayne, M. Jochum, W. G. Large, S. Peacock, and S. G. Yeager. 2012. The CCSM4 ocean component. J. Clim. **25:** 1361-1389. doi:10.1175/JCLI-D-11-00091.1

Dever, E. P., C. E. Dorman, and J. L. Largier. 2006. Surface boundary-layer variability off Northern California, USA, during upwelling. Deep Sea Res. Part II **53:** 2887-2905. doi:10.1016/j.dsr2.2006.09.001

Durant, J. M., D. Ø. Hjermann, G. Ottersen, and N. C. Stenseth. 2007. Climate and the match or mismatch between predator requirements and resource availability. Clim. Res. **33:** 271-283. doi:10.3354/cr033271

Eppley, R. W. 1972. Temperature and phytoplankton growth in the sea. Fish. Bull. **70:** 1063-1085.

Evans, G. T., and J. S. Parslow. 1985. A Model of Annual Plankton Cycles. Biological Oceanography **3:** 327-347. doi:10.1080/01965581.1985.10749478

Falkowski, P. G., R. T. Barber, and V. Smetacek. 1998. Biogeochemical controls and feedbacks on ocean primary production. Science **281:** 200-206. doi:10.1126/science.281.5374.200

Fernández, E., and A. Bode. 1994. Succession of phytoplankton assemblages in relation to the hydrography in the southern Bay of Biscay: a multivariate approach. Sci. Mar. **58:** 191-205. http://www.icm.csic.es/scimar/index.php/secId/196/IdArt/2688/.

Ferrari, R., S. T. Merrifield, and J. R. Taylor. 2015. Shutdown of convection triggers increase of surface chlorophyll. J. Mar. Syst. **147:** 116-122. doi:10.1016/j.jmarsys.2014.02.009

Ferreira, A. S. A., H. Hátún, F. Counillon, M. R. Payne, and A. W. Visser. 2015. Synoptic-scale analysis of mechanisms driving surface chlorophyll dynamics in the North Atlantic. Biogeosciences **12:** 3641-3653. doi:10.5194/bg-12-3641-2015

Fischer, A., E. Moberg, H. Alexander, E. Brownlee, K. Hunter-Cevera, K. Pitz, S. Rosengard, and H. Sosik. 2014. Sixty years of Sverdrup: a retrospective of progress in the study of phytoplankton blooms. Oceanography **27:** 222–235. doi:10.5670/oceanog.2014.26

Follows, M., and S. Dutkiewicz. 2002. Meteorological modulation of the North Atlantic spring bloom. Deep Sea Res. Part II **49:** 321-344. doi:10.1016/S0967-0645(01)00105-9

Franks, P. J. S. 2015. Has Sverdrup's critical depth hypothesis been tested? Mixed layers vs. turbulent layers. ICES J. Mar. Sci. **72:** 1897-1907. doi:10.1093/icesjms/fsu175

González-Gil, R., F. G. Taboada, J. Höfer, and R. Anadón. 2015. Winter mixing and coastal upwelling drive long-term changes in zooplankton in the Bay of Biscay (1993–2010). J. Plankton Res. **37:** 337-351. doi:10.1093/plankt/fbv001

González Taboada, F., and R. Anadón. 2014. Seasonality of North Atlantic phytoplankton from space: impact of environmental forcing on a changing phenology (1998–2012). Glob. Change Biol. **20:** 698-712. doi:10.1111/gcb.12352

Hartman, S. E., M. C. Hartman, D. J. Hydes, Z.-P. Jiang, D. Smythe-Wright, and C. González-Pola. 2013. Seasonal and inter-annual variability in nutrient supply in relation to mixing in the Bay of Biscay. Deep Sea Res. Part II **57:** 1303-1312. doi:10.1016/j.dsr2.2013.09.032

Hastie, T. J., and R. J. Tibshirani. 1990. Generalized additive models. Chapman & Hall/CRC.

683 Henson, S. A., J. P. Dunne, and J. L. Sarmiento. 2009. Decadal variability in North
684 Atlantic phytoplankton blooms. J. Geophys. Res.: Oceans **114:** C04013.
685 doi:10.1029/2008JC005139

686 Henson, S. A., I. Robinson, J. T. Allen, and J. J. Waniek. 2006. Effect of meteorological
687 conditions on interannual variability in timing and magnitude of the spring bloom
688 in the Irminger Basin, North Atlantic. Deep Sea Res. Part I **53:** 1601-1615.
689 doi:10.1016/j.dsr.2006.07.009

690 Henson, S. A., J. L. Sarmiento, J. P. Dunne, L. Bopp, I. Lima, S. C. Doney, J. John, and
691 C. Beaulieu. 2010. Detection of anthropogenic climate change in satellite records
692 of ocean chlorophyll and productivity. Biogeosciences **7:** 621-640.
693 doi:10.5194/bg-7-621-2010

694 Hjort, J. 1914. Fluctuations in the great fisheries of northern Europe viewed in the light
695 of biological research. Rapp. P.-V. Reún. Cons. Intern. Explor. Mer. **20:** 1-228.

696 Houpert, L., P. Testor, X. D. de Madron, S. Somot, F. D'Ortenzio, C. Estournel, and H.
697 Lavigne. 2015. Seasonal cycle of the mixed layer, the seasonal thermocline and
698 the upper-ocean heat storage rate in the Mediterranean Sea derived from
699 observations. Prog. Oceanogr. **132:** 333-352. doi:10.1016/j.pocean.2014.11.004

700 Huisman, J., P. van Oostveen, and F. J. Weissing. 1999. Critical depth and critical
701 turbulence: two different mechanisms for the development of phytoplankton
702 blooms. Limnol. Oceanogr. **44:** 1781-1787. doi:10.4319/lo.1999.44.7.1781

703 Hurrell, J. W., and C. Deser. 2009. North Atlantic climate variability: The role of the
704 North Atlantic Oscillation. J. Mar. Syst. **78:** 28-41.
705 doi:10.1016/j.jmarsys.2008.11.026

706 Ikeda, T. 1985. Metabolic rates of epipelagic marine zooplankton as a function of body
707 mass and temperature. Mar. Biol. **85:** 1-11. doi:10.1007/BF00396409

708 Ji, R., M. Edwards, D. L. Mackas, J. A. Runge, and A. C. Thomas. 2010. Marine plankton
709 phenology and life history in a changing climate: current research and future
710 directions. J. Plankton Res. **32:** 1355-1368. doi:10.1093/plankt/fbq062

711 Karl, D. M. 2010. Oceanic ecosystem time-series programs: Ten lessons learned.
712 Oceanography **23:** 104-125. doi:10.5670/oceanog.2010.27

713 Klausmeier, C. A., and E. Litchman. 2001. Algal games: The vertical distribution of
714 phytoplankton in poorly mixed water columns. Limnol. Oceanogr. **46:** 1998-
715 2007. doi:10.4319/lo.2001.46.8.1998

716 Koeller, P. and others. 2009. Basin-scale coherence in phenology of shrimps and
717 phytoplankton in the North Atlantic Ocean. Science **324:** 791-793.
718 doi:10.1126/science.1170987

719 Körtzinger, A., W. Koeve, P. Kähler, and L. Mintrop. 2001. C : N ratios in the mixed
720 layer during the productive season in the northeast Atlantic Ocean. Deep Sea Res.
721 Part I **48:** 661-688. doi:https://doi.org/10.1016/S0967-0637(00)00051-0

722 Kristiansen, T., K. F. Drinkwater, R. G. Lough, and S. Sundby. 2011. Recruitment
723 variability in North Atlantic cod and match-mismatch dynamics. PLoS One **6:**
724 e17456. doi:10.1371/journal.pone.0017456

725 Lampitt, R. S. 1985. Evidence for the seasonal deposition of detritus to the deep-sea floor
726 and its subsequent resuspension. Deep-Sea Res. Part A Oceanogr. Res. Pap. **32:**
727 885-897. doi:10.1016/0198-0149(85)90034-2

728 Levitus, S. and others. 2012. World ocean heat content and thermosteric sea level change
729 (0–2000 m), 1955–2010. Geophys. Res. Lett. **39:** L10603.
730 doi:10.1029/2012GL051106

731 Lindemann, C., and M. A. St. John. 2014. A seasonal diary of phytoplankton in the North
732 Atlantic. Front. Mar. Sci. **1:** 1-6. doi:10.3389/fmars.2014.00037

733 Longhurst, A. R., and W. G. Harrison. 1989. The biological pump: profiles of plankton
734 production and consumption in the upper ocean. Prog. Oceanogr. **22:** 47-123.
735 doi:10.1016/0079-6611(89)90010-4

736 Llope, M., R. Anadón, J. Á. Sostres, and L. Viesca. 2007. Nutrients dynamics in the
737 southern Bay of Biscay (1993–2003): winter supply, stoichiometry, long-term
738 trends, and their effects on the phytoplankton community. J. Geophys. Res.:
739 Oceans **112:** C07029. doi:10.1029/2006JC003573

740 Llope, M., R. Anadón, L. Viesca, M. Quevedo, R. González-Quirós, and N. C. Stenseth.
741 2006. Hydrography of the southern Bay of Biscay shelf-break region: integrating
742 the multiscale physical variability over the period 1993-2003. J. Geophys. Res.:
743 Oceans **111:** C09021. doi:10.1029/2005JC002963

744 Mann, K. H., and J. R. N. Lazier. 2006. Dynamics of marine ecosystems. Biological–
745 Physical Interactions in the Oceans, 3rd ed. Blackwell.

746 Martinez, E., D. Antoine, F. D'Ortenzio, and C. de Boyer Montégut. 2011. Phytoplankton
747 spring and fall blooms in the North Atlantic in the 1980s and 2000s. J. Geophys.
748 Res.: Oceans **116:** C11029. doi:10.1029/2010JC006836

749 McClain, C. R. 2009. A decade of satellite ocean color observations. Annu. Rev. Mar.
750 Sci. **1:** 19-42. doi:10.1146/annurev.marine.010908.163650

751 Monterey, G. I., and S. Levitus. 1997. Seasonal variability of mixed layer depth for the
752 World Ocean. NOAA Atlas NESDIS 14, US Government Printing Office.

753 Moore, C. M. and others. 2013. Processes and patterns of oceanic nutrient limitation. Nat.
754 Geosci. **6:** 701-710. doi:10.1038/ngeo1765

755 NASA Goddard Space Flight Center, Ocean Ecology Laboratory, Ocean Biology
756 Processing Group (OBPG). 2015a. Moderate-resolution Imaging
757 Spectroradiometer (MODIS) Aqua Chlorophyll Data; 2013.1.1 Reprocessing.
758 NASA OB.DAAC, Greenbelt, MD, USA.
759 doi:10.5067/AQUA/MODIS/L3M/CHL/2014. Accessed on 2015/01/09.

760 NASA Goddard Space Flight Center, Ocean Ecology Laboratory, Ocean Biology
761 Processing Group (OBPG). 2015b. Sea-viewing Wide Field-of-view Sensor
762 (SeaWiFS) Chlorophyll Data; 2010.0 Reprocessing. NASA OB.DAAC,
763 Greenbelt, MD, USA. doi:10.5067/AQUA/MODIS/L3M/CHL/2014. Accessed
764 on 2015/01/09.

765

766 Nychka, D., S. Bandyopadhyay, D. Hammerling, F. Lindgren, and S. Sain. 2015. A
767 Multiresolution Gaussian Process Model for the Analysis of Large Spatial
768 Datasets. J. Comput. Graph. Stat. **24:** 579-599.
769 doi:10.1080/10618600.2014.914946

770 Nychka, D., D. Hammerling, S. Sain, and N. Lenssen. 2016. LatticeKrig: Multiresolution
771 Kriging Based on Markov Random Fields. R package version 6.2:
772 www.image.ucar.edu/LatticeKrig. doi: 10.5065/D6HD7T1R.

773

774 O'Reilly, J. E. and others. 2000. Ocean color chlorophyll a algorithms for SeaWiFS, OC2,
775 and OC4: Version 4, p. 9-23. *In* S. B. Hooker and E. R. Firestone [eds.], SeaWiFS
776 Postlaunched Calibration and Validation Analyses, Part 3. NASA Tech. Memo
777 2000-206892,Vol. 11. NASA, GoddardSpace Flight Center.

778 Parsons, T. R., and C. M. Lalli. 1988. Comparative oceanic ecology of the plankton
779 communities of the subarctic Atlantic and Pacific oceans. Oceanogr. Mar. Biol.
780 Annu. Rev. **26:** 317-359.

781 Platt, T., C. Fuentes-Yaco, and K. T. Frank. 2003. Spring algal bloom and larval fish
782 survival. Nature **423:** 398-399. doi:10.1038/423398b

783 R Core Team. 2017. R: A language and environment for statistical computing. R
784 Foundation for Statistical Computing, Vienna, Austria. Available from
785 http://www.R-project.org/.

786

787 Racault, M.-F., C. Le Quéré, E. Buitenhuis, S. Sathyendranath, and T. Platt. 2012.
788 Phytoplankton phenology in the global ocean. Ecol. Indicators **14:** 152-163.
789 doi:10.1016/j.ecolind.2011.07.010

790 Rantajärvi, E., R. Olsonen, S. Hällfors, J.-M. Leppänen, and M. Raateoja. 1998. Effect of
791 sampling frequency on detection of natural variability in phytoplankton:
792 unattended high-frequency measurements on board ferries in the Baltic Sea. ICES
793 J. Mar. Sci. **55:** 697-704. doi:10.1006/jmsc.1998.0384

794 Redfield, A. C. 1958. The biological control of chemical factors in the environment. Am.
795 Sci. **46:** 230A-221.

796 Reynolds, C. S. 2006. The ecology of phytoplankton. Cambridge University Press.

797 Reynolds, R. W., T. M. Smith, C. Liu, D. B. Chelton, K. S. Casey, and M. G. Schlax.
798 2007. Daily high-resolution-blended analyses for sea surface temperature. J. Clim.
799 **20:** 5473-5496. doi:10.1175/2007JCLI1824.1

800 RStudio Team. 2016. RStudio: Integrated Development Environment for R. RStudio,
801 Inc., Boston, MA. Avialable from http://www.rstudio.com.

802

803 Rumín-Caparrós, A., A. Sanchez-Vidal, C. González-Pola, G. Lastras, A. Calafat, and M.
804 Canals. 2016. Particle fluxes and their drivers in the Avilés submarine canyon and
805 adjacent slope, central Cantabrian margin, Bay of Biscay. Prog. Oceanogr. **144:**
806 39-61. doi:https://doi.org/10.1016/j.pocean.2016.03.004

807 Sambrotto, R. N., H. J. Niebauer, J. J. Goering, and R. L. Iverson. 1986. Relationships
808 among vertical mixing, nitrate uptake, and phytoplankton growth during the
809 spring bloom in the southeast Bering Sea middle shelf. Cont. Shelf Res. **5:** 161-
810 198. doi:10.1016/0278-4343(86)90014-2

811 Sanders, R. and others. 2014. The biological carbon pump in the North Atlantic. Prog.
812 Oceanogr. **129:** 200-218. doi:10.1016/j.pocean.2014.05.005

813 Sarmiento, J. L., and N. Gruber. 2006. Ocean biogeochemical dynamics. Princeton
814 University Press.

815 Siegel, D. A., S. C. Doney, and J. A. Yoder. 2002. The North Atlantic spring
816 phytoplankton bloom and Sverdrup's critical depth hypothesis. Science **296:** 730-
817 733. doi:10.1126/science.1069174

818 Sieracki, M. E., P. G. Verity, and D. K. Stoecker. 1993. Plankton community response to
819 sequential silicate and nitrate depletion during the 1989 North Atlantic spring
820 bloom. Deep Sea Res. Part II **40:** 213-225. doi:10.1016/0967-0645(93)90014-E

821 Smayda, T. J. 1970. The suspension and sinking of phytoplankton in the sea. Oceanogr.
822 Mar. Biol. Annu. Rev. **8:** 353-414. doi:10.1002/iroh.19720570110

823 Smetacek, V. S. 1985. Role of sinking in diatom life-history cycles: ecological,
824 evolutionary and geological significance. Mar. Biol. **84:** 239-251.
825 doi:10.1007/BF00392493

826 Somavilla Cabrillo, R., C. González-Pola, M. Ruiz-Villarreal, and A. Lavín Montero.
827 2011. Mixed layer depth (MLD) variability in the southern Bay of Biscay.
828 Deepening of winter MLDs concurrent with generalized upper water warming
829 trends? Ocean. Dynam. **61:** 1215-1235. doi:10.1007/s10236-011-0407-6

830 Somavilla, R., C. González-Pola, C. Rodriguez, S. A. Josey, R. F. Sánchez, and A. Lavín.
831 2009. Large changes in the hydrographic structure of the Bay of Biscay after the
832 extreme mixing of winter 2005. J. Geophys. Res.: Oceans **114:** C01001.
833 doi:10.1029/2008JC004974

Sverdrup, H. U. 1953. On conditions for the Vernal Blooming of Phytoplankton. J. Cons. Int. Explor. Mer. **18:** 287-295. doi:10.1093/icesjms/18.3.287

Taboada, F. G., and R. Anadón. 2012. Patterns of change in sea surface temperature in the North Atlantic during the last three decades: beyond mean trends. Clim. Change **115:** 419-431. doi:10.1007/s10584-012-0485-6

Taylor, J. R., and R. Ferrari. 2011. Shutdown of turbulent convection as a new criterion for the onset of spring phytoplankton blooms. Limnol. Oceanogr. **56:** 2293-2307. doi:10.4319/lo.2011.56.6.2293

Townsend, D. W., L. M. Cammen, P. M. Holligan, D. E. Campbell, and N. R. Pettigrew. 1994. Causes and consequences of variability in the timing of spring phytoplankton blooms. Deep Sea Res. Part I **41:** 747-765. doi:10.1016/0967-0637(94)90075-2

Ueyama, R., and B. C. Monger. 2005. Wind-induced modulation of seasonal phytoplankton blooms in the North Atlantic derived from satellite observations. Limnol. Oceanogr. **50:** 1820-1829. doi:10.4319/lo.2005.50.6.1820

Valdés, L., A. Lavín, M. L. Fernández de Puelles, M. Varela, R. Anadón, A. Miranda, J. Camiñas, and J. Mas. 2002. Spanish Ocean Observation System. IEO Core Project: studies on time series of oceanographic data. Elsevier Oceanogr. Ser. **66:** 99-105. doi:10.1016/S0422-9894(02)80014-9

Valdés, L. and others. 2007. A decade of sampling in the Bay of Biscay: What are the zooplankton time series telling us? Prog. Oceanogr. **74:** 98-114. doi:10.1016/j.pocean.2007.04.016

Varela, M. 1996. Phytoplankton ecology in the Bay of Biscay. Sci. Mar. **60:** 45-53.

Wickham, H. 2009. ggplot2: elegant graphics for data analysis. Springer.

Williams, R. G., and M. J. Follows. 2003. Physical transport of nutrients and the maintenance of biological production, p. 19-51. *In* M. J. R. Fasham [ed.], Ocean Biogeochemistry: The Role of the Ocean Carbon Cycle in Global Change. Springer.

Wood, S. N. 2006. Generalized additive models: an introduction with R. Chapman and Hall/CRC.

Wood, S. N., F. Scheipl, and J. J. Faraway. 2013. Straightforward intermediate rank tensor product smoothing in mixed models. Stat. Comput. **23:** 341-360. doi:10.1007/s11222-012-9314-z

Yentsch, C. S., and D. W. Menzel. 1963. A method for the determination of phytoplankton chlorophyll and phaeophytin by fluorescence. Deep-Sea Res. Oceanogr. Abstr. **10:** 221-231. doi:10.1016/0011-7471(63)90358-9

870 Yoder, J. A., C. R. McClain, G. C. Feldman, and W. E. Esaias. 1993. Annual cycles of
871 phytoplankton chlorophyll concentrations in the global ocean: A satellite view.
872 Glob. Biogeochem. Cycles **7:** 181-193. doi:10.1029/93GB02358

873 Yoshie, N., Y. Yamanaka, M. J. Kishi, and H. Saito. 2003. One dimensional ecosystem
874 model simulation of the effects of vertical dilution by the winter mixing on the
875 spring diatom bloom. J. Oceanogr. **59:** 563-571.
876 doi:10.1023/B:JOCE.0000009586.02554.d3

877

878 **Acknowledgments**

879 We thank all the people that helped in the establishment and maintenance of the time
880 series collected at station E3 (Cudillero Transect), especially those from the Areas of
881 Ecology and Zoology of the University of Oviedo and the entire crew from the research
882 vessel José Rioja. We also thank NASA Ocean Biology Processing Group (OBPG) and
883 NOAA National Climatic Data Center (NCDC) for the production, availability and
884 maintenance of the remote sensing data analyzed in this work. We are especially grateful
885 to D. Tommasi, A. Rivera and S. Romero for their useful comments. Cudillero time series
886 are part of the project RADIALES, Instituto Español de Oceanografía (IEO). This is a
887 contribution of the Asturias Marine Observatory.

888 This research was co-funded by the agreement "Control a largo plazo de las
889 condiciones químico-biológicas de la Plataforma Continental de Asturias" [Instituto
890 Español de Oceanografía (IEO) and University of Oviedo] and by the project DOS
891 MARES (CTM2010-21810- C03-02, Ministerio de Economía y Competitividad,
892 Gobierno de España). R.G.-G. was supported by a FPU fellowship from the Ministerio
893 de Educación, Cultura y Deporte, Gobierno de España.

894 **Figures**

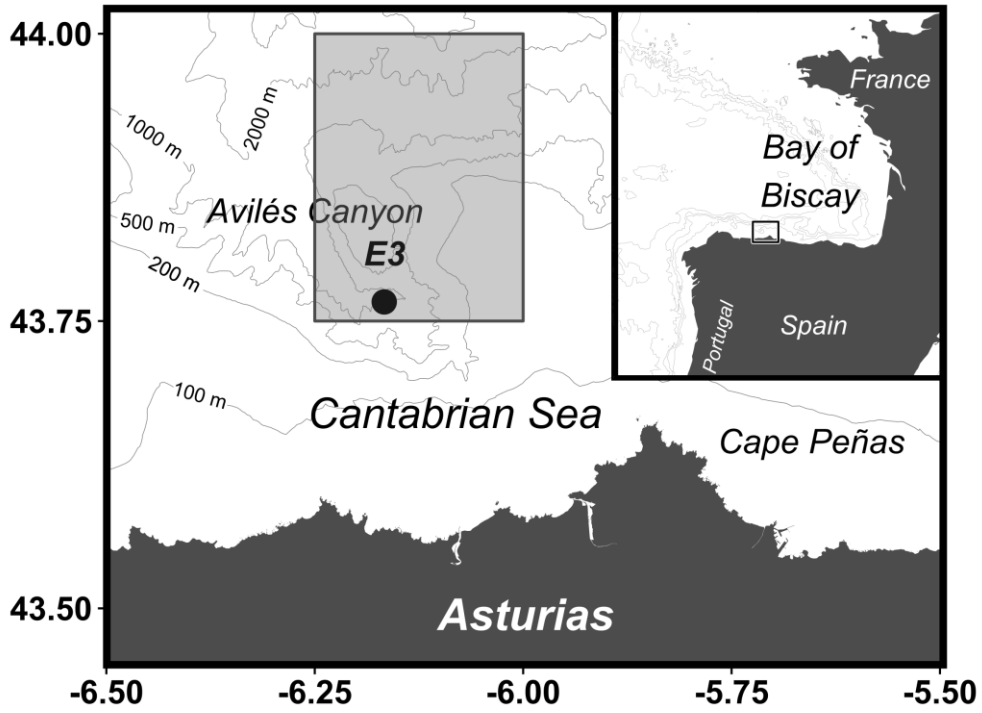


**Fig. 1.** Map of the study area in the central Cantabrian Sea and its position in the Bay of Biscay. The shaded region around station E3 (dot) corresponds to the 0.25º x 0.25º quadrangle used to average satellite data.

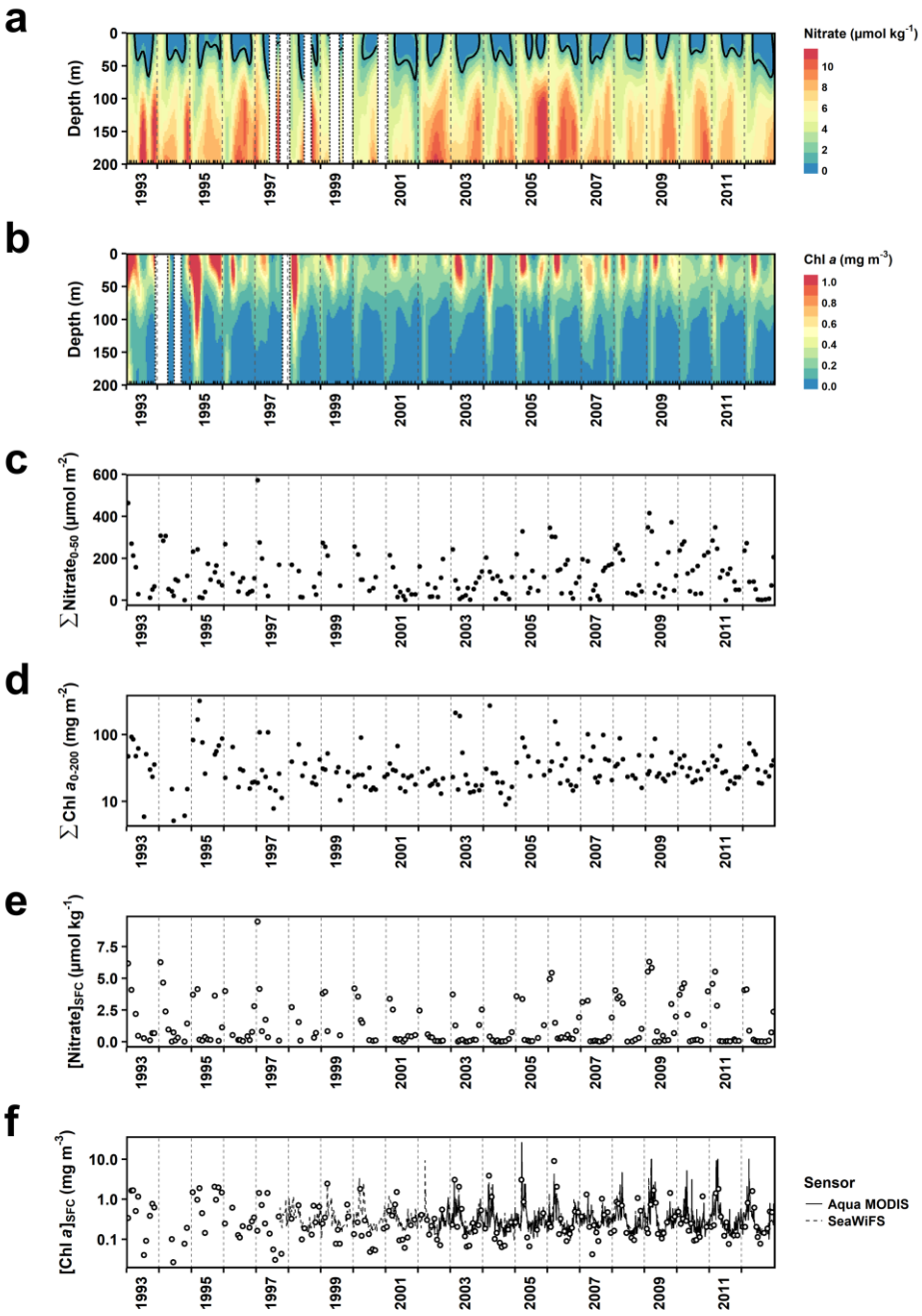


**Fig. 2.** Intra- and interannual variations in: **(a)** nitrate and **(b)** Chl *a* concentrations over the uppermost 200 m of the water column interpolated using kriging techniques, **(c)** depth-integrated nitrate (0-50 m, $\Sigma Nitrate_{0\text{-}50}$), **(d)** depth-integrated Chl *a* (0-200 m, $\Sigma Chl\ a_{0\text{-}200}$), **(e)** surface nitrate concentration ($[Nitrate]_{SFC}$) and **(f)** surface Chl *a* concentration ($[Chl\ a]_{SFC}$) from in situ (dots) and satellite (lines) observations. In all panels, years are separated by gray vertical dashed lines. In **(a)** and **(b)**, inner tick marks on the x-axis indicate those dates when data were collected, and data gaps spanning three or more consecutive months appear as blank stripes delimited by vertical dotted lines. The thick contour line in **(a)** denotes the 1 µmol $kg^{-1}$ nitrate isoline (i.e. the nitracline). Note the use of a $log_{10}$ scale for Chl *a* in panels **(d)** and **(f)**.

895

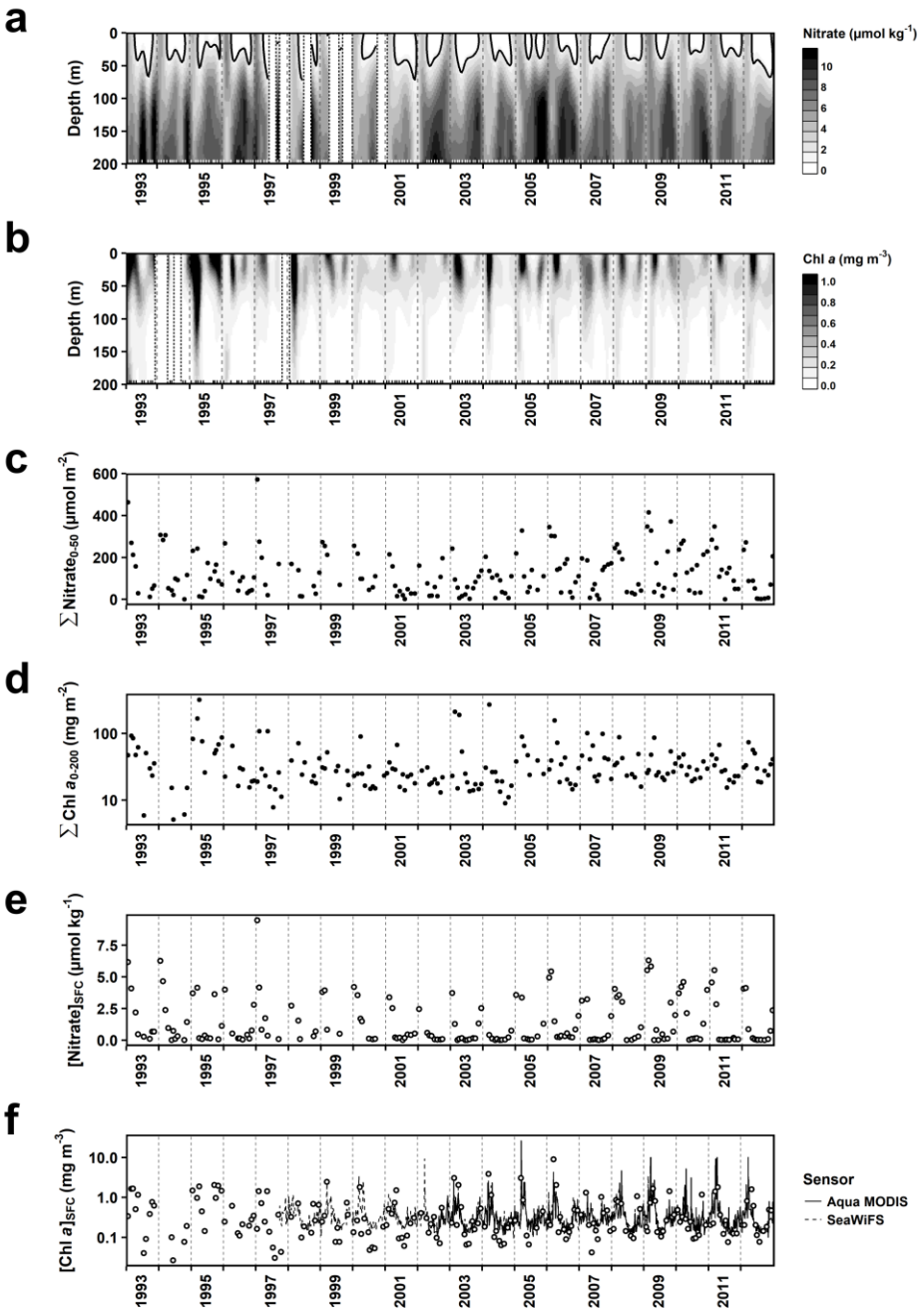


**Fig. 2 (b/w).** Intra- and interannual variations in: **(a)** nitrate and **(b)** Chl *a* concentrations over the uppermost 200 m of the water column interpolated using kriging techniques, **(c)** depth-integrated nitrate (0-50 m, $\Sigma Nitrate_{0\text{-}50}$), **(d)** depth-integrated Chl *a* (0-200 m, $\Sigma Chl\ a_{0\text{-}200}$), **(e)** surface nitrate concentration ($[Nitrate]_{SFC}$) and **(f)** surface Chl *a* concentration ($[Chl\ a]_{SFC}$) from in situ (dots) and satellite (lines) observations. In all panels, years are separated by gray vertical dashed lines. In **(a)** and **(b)**, inner tick marks on the x-axis indicate those dates when data were collected, and data gaps spanning three or more consecutive months appear as blank stripes delimited by vertical dotted lines. The thick contour line in **(a)** denotes the 1 µmol $kg^{-1}$ nitrate isoline (i.e. the nitracline). Note the use of a $log_{10}$ scale for Chl *a* in panels **(d)** and **(f)**.

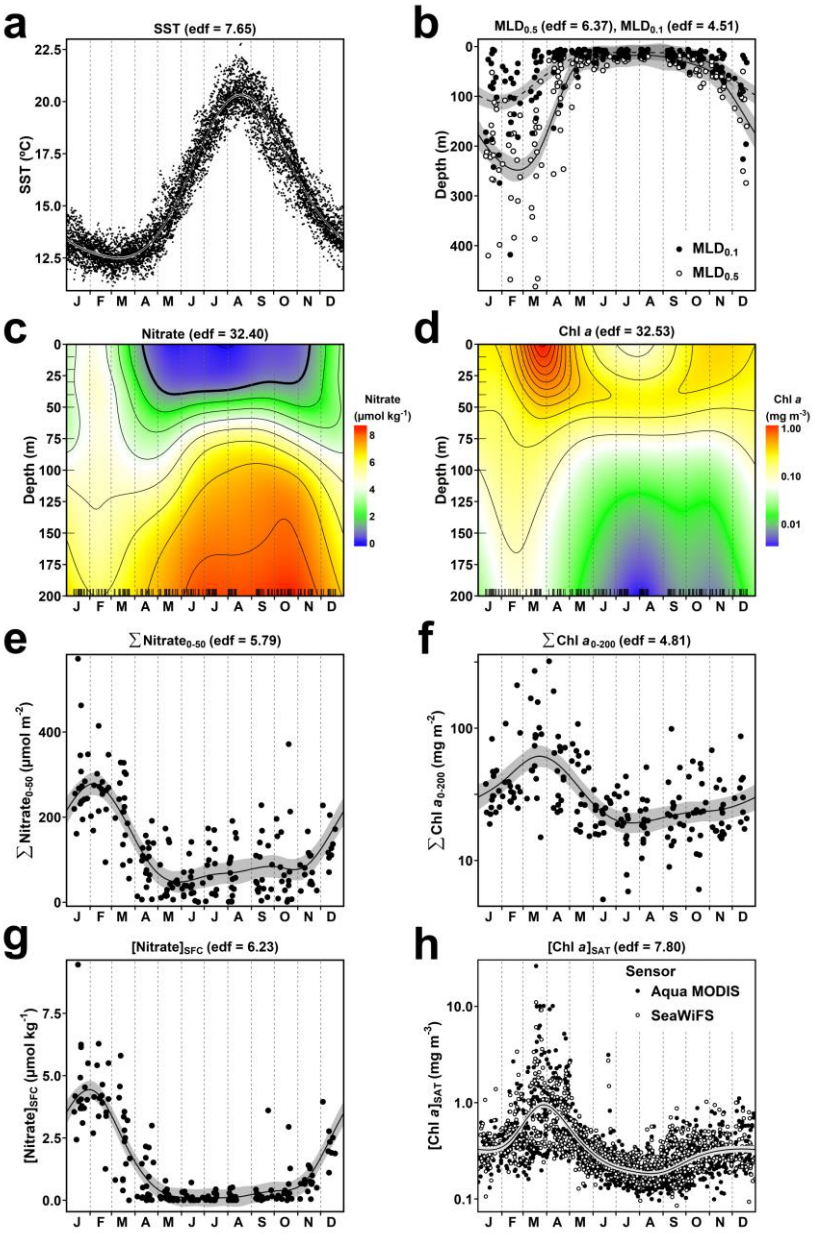


**Fig. 3.** Seasonality of: **(a)** sea surface temperature (SST) based on satellite retrievals, **(b)** mixed layer depth (MLD) calculated using two different criteria (see *Material and methods*), **(c)** nitrate and **(d)** Chl *a* concentration over the first 200 m of the water column, **(e)** depth-integrated nitrate (0-50 m, $\Sigma Nitrate_{0\text{-}50}$), **(f)** depth-integrated Chl *a* (0-200 m, $\Sigma Chl\ a_{0\text{-}200}$), **(g)** surface nitrate concentration ($[Nitrate]_{SFC}$) and **(h)** surface satellite Chl *a* concentration ($[Chl\ a]_{SAT}$). Observed concentrations or integrated values (dots) and estimated seasonal cycles (solid lines in **a-b** and **e-h** or contour plots in **c-d**) are shown. In **(a-b)** and **(e-h)**, the 95% confidence intervals (shaded areas) associated with the estimated seasonal cycles are shown. Predicted values for each variable are based on the output of the generalized additive models (GAMs). The estimated degrees of freedom (edf) for each model are indicated. The inner tick marks on each axis in **(c)** and **(d)** indicate where data were available. The thick contour line in **(c)** denotes the 1 μmol $kg^{-1}$ nitrate isoline (i.e. the nitracline). Note the use of a $log_{10}$ scale for Chl *a*.

897

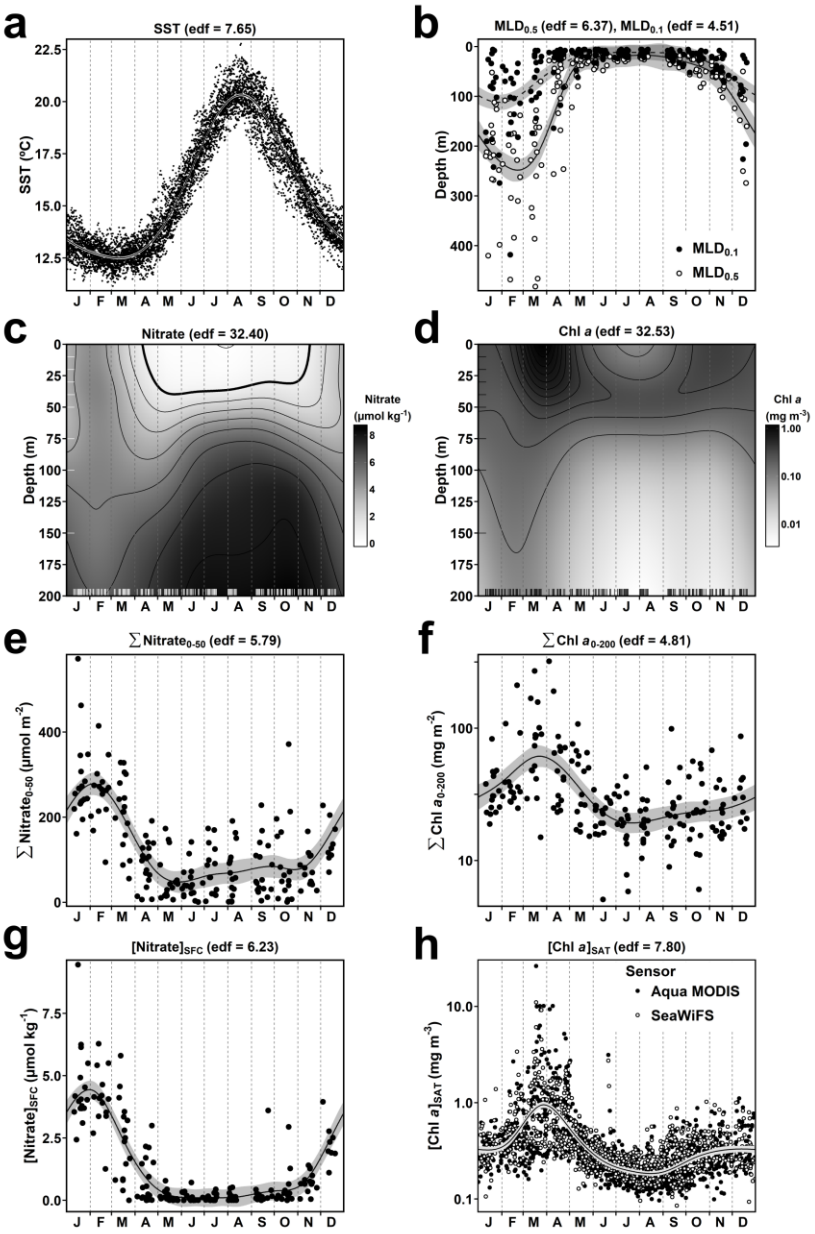


**Fig. 3 (b/w).** Seasonality of: **(a)** sea surface temperature (SST) based on satellite retrievals, **(b)** mixed layer depth (MLD) calculated using two different criteria (see *Material and methods*), **(c)** nitrate and **(d)** Chl *a* concentration over the first 200 m of the water column, **(e)** depth-integrated nitrate (0-50 m, $\Sigma Nitrate_{0\text{-}50}$), **(f)** depth-integrated Chl *a* (0-200 m, $\Sigma Chl\ a_{0\text{-}200}$), **(g)** surface nitrate concentration ($[Nitrate]_{SFC}$) and **(h)** surface satellite Chl *a* concentration ($[Chl\ a]_{SAT}$). Observed concentrations or integrated values (dots) and estimated seasonal cycles (solid lines in **a-b** and **e-h** or contour plots in **c-d**) are shown. In **(a-b)** and **(e-h)**, the 95% confidence intervals (shaded areas) associated with the estimated seasonal cycles are shown. Predicted values for each variable are based on the output of the generalized additive models (GAMs). The estimated degrees of freedom (edf) for each model are indicated. The inner tick marks on each axis in **(c)** and **(d)** indicate where data were available. The thick contour line in **(c)** denotes the 1 μmol $kg^{-1}$ nitrate isoline (i.e. the nitracline). Note the use of a $\log_{10}$ scale for Chl *a*.

898

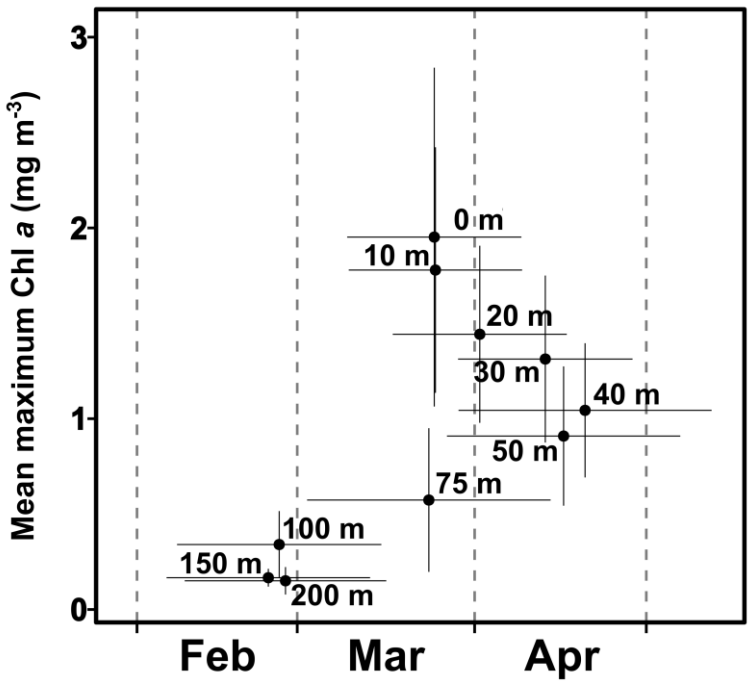


**Fig. 4.** Mean maximum Chl *a* concentration for each depth during the first half of the year and corresponding mean day of occurrence. Error bars indicate the 95 % confidence interval. Months are delimited by vertical dashed lines.

899

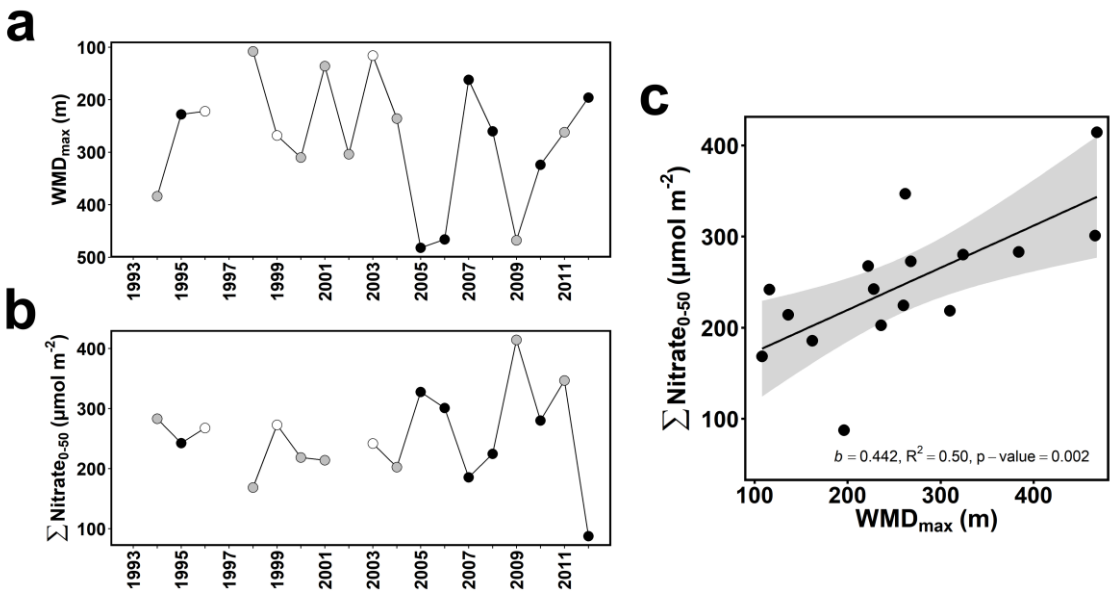


**Fig. 5.** Inter-annual variations of **(a)** maximum winter mixing depth ($WMD_{max}$) and **(b)** depth-integrated nitrate (0-50 m, $\Sigma Nitrate_{0\text{-}50}$) at the $WMD_{max}$ sampling date. Dot color represents the winter month when $WMD_{max}$ was measured (white, January; gray, February; black, March). **(c)** Linear relationship between $\Sigma Nitrate_{0\text{-}50}$ at the $WMD_{max}$ sampling date and $WMD_{max}$. The shaded area represents the 95% confidence interval associated to the linear correlation. The slope (*b*), proportion of variance explained ($R^2$) and p-value of the relationship are shown.

900

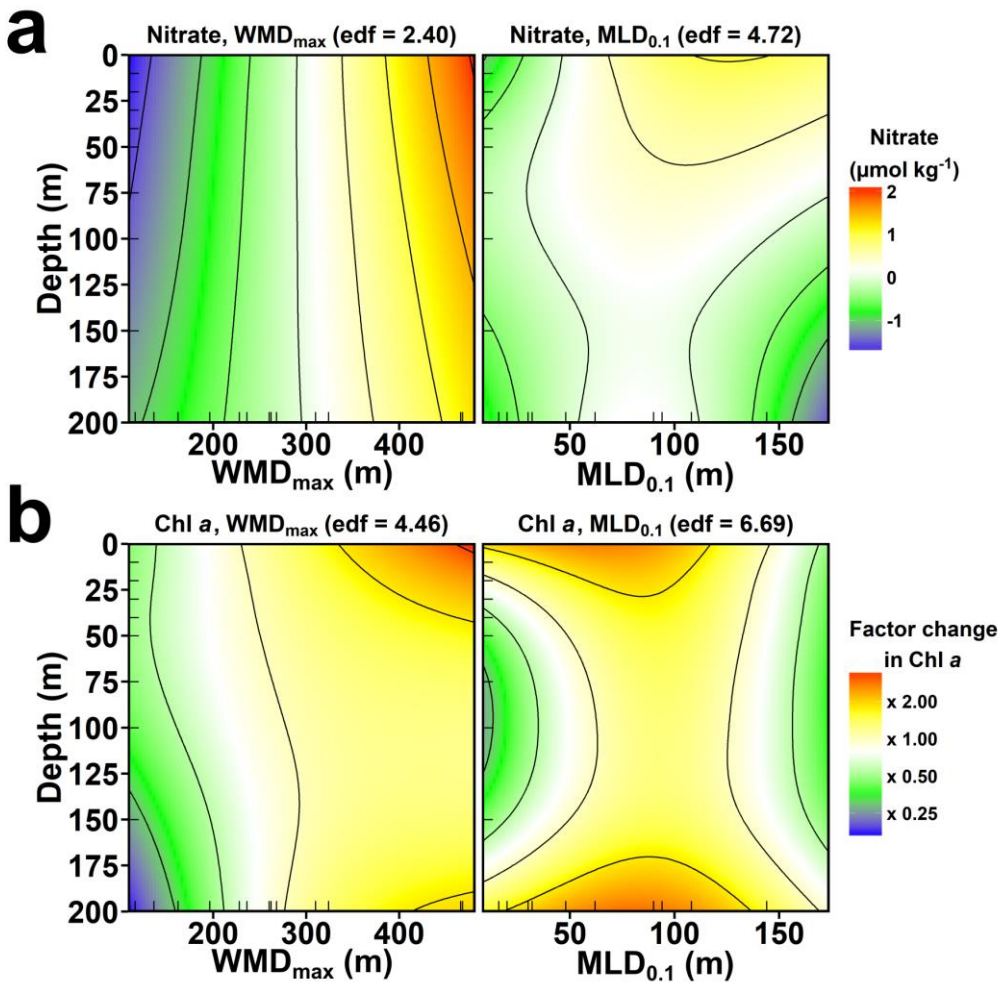


**Fig. 6.** Predicted **(a)** additive effects on nitrate concentration and **(b)** multiplicative effects on Chl *a* concentration of both maximum winter mixing depth ($WMD_{max}$) and near-surface stratification ($MLD_{0.1}$) in March. These values were obtained based on the best generalized additive model (GAM) of a set of proposed models to explore the effect of $WMD_{max}$ and $MLD_{0.1}$ on nitrate and Chl *a* concentrations (see Table 1). All terms in the model had a p-value < 0.010 or < 0.050 for nitrate and Chl *a* concentration, respectively. The estimated degrees of freedom (edf) are also shown. The inner tick marks on each axis indicate where data were available.

901

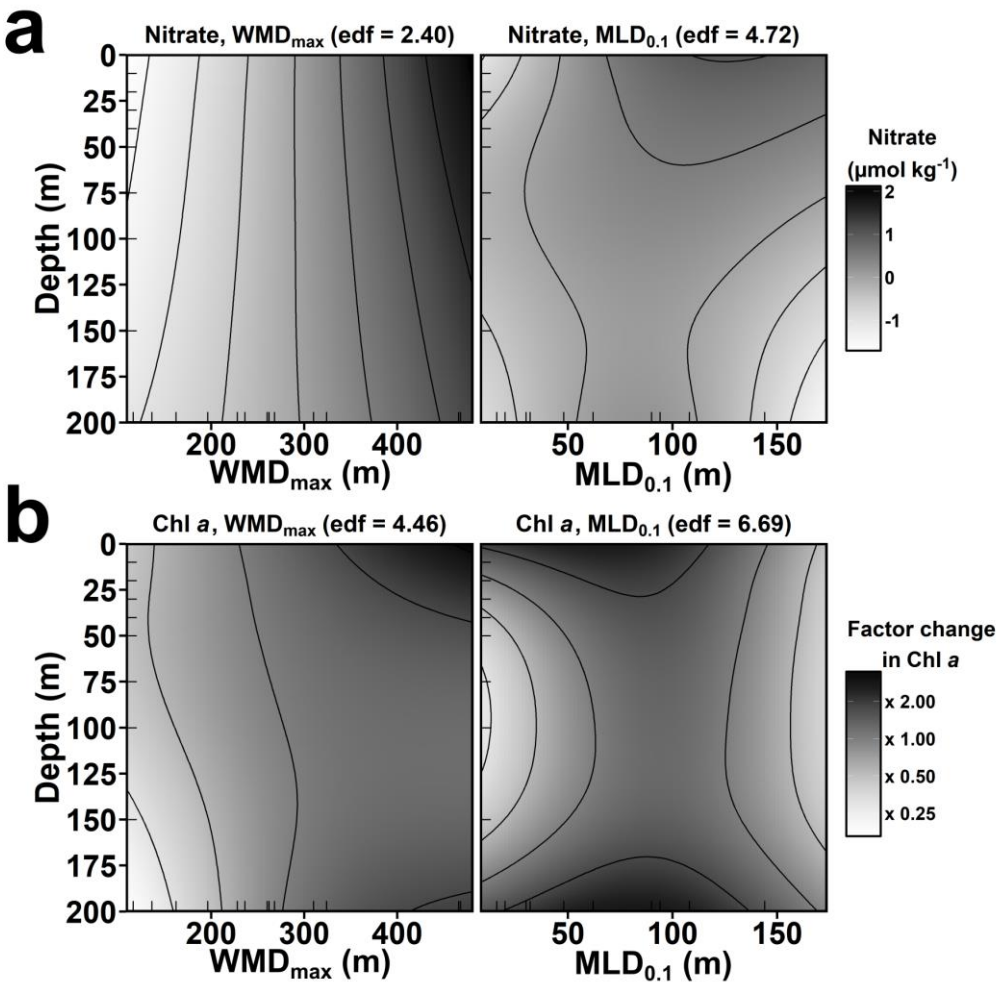


**Fig. 6 (b/w).** Predicted **(a)** additive effects on nitrate concentration and **(b)** multiplicative effects on Chl *a* concentration of both maximum winter mixing depth ($WMD_{max}$) and near-surface stratification ($MLD_{0.1}$) in March. These values were obtained based on the best generalized additive model (GAM) of a set of proposed models to explore the effect of $WMD_{max}$ and $MLD_{0.1}$ on nitrate and Chl *a* concentrations (see Table 1). All terms in the model had a p-value < 0.010 or < 0.050 for nitrate and Chl *a* concentration, respectively. The estimated degrees of freedom (edf) are also shown. The inner tick marks on each axis indicate where data were available.

902

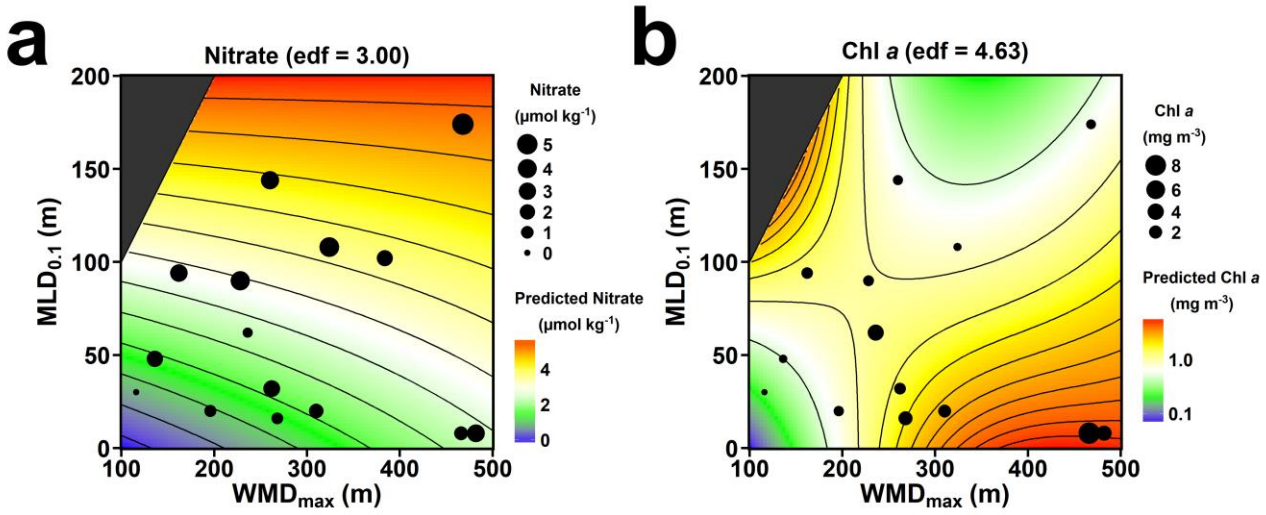


**Fig. 7.** Observed (dot size) and predicted (contour plot) concentrations of **(a)** nitrate and **(b)** Chl *a* at surface (~ 0 m depth) in March. Predicted values were obtained based on the generalized additive model (GAM) in Table 2 that included an interaction term between the maximum winter mixing depth ($WMD_{max}$) and the near-surface stratification depth ($MLD_{0.1}$) in March. This interaction term had a p-value < 0.010 or < 0.050 for nitrate and Chl *a* concentration, respectively. The estimated degrees of freedom (edf) for each model are indicated. The dark gray triangles on the top left corners delimit those combinations of $WMD_{max}$ and $MLD_{0.1}$ that are not possible ($WMD_{max}$ cannot be shallower than $MLD_{0.1}$). Note that predicted Chl *a* concentrations are shown in $log_{10}$ scale.

903

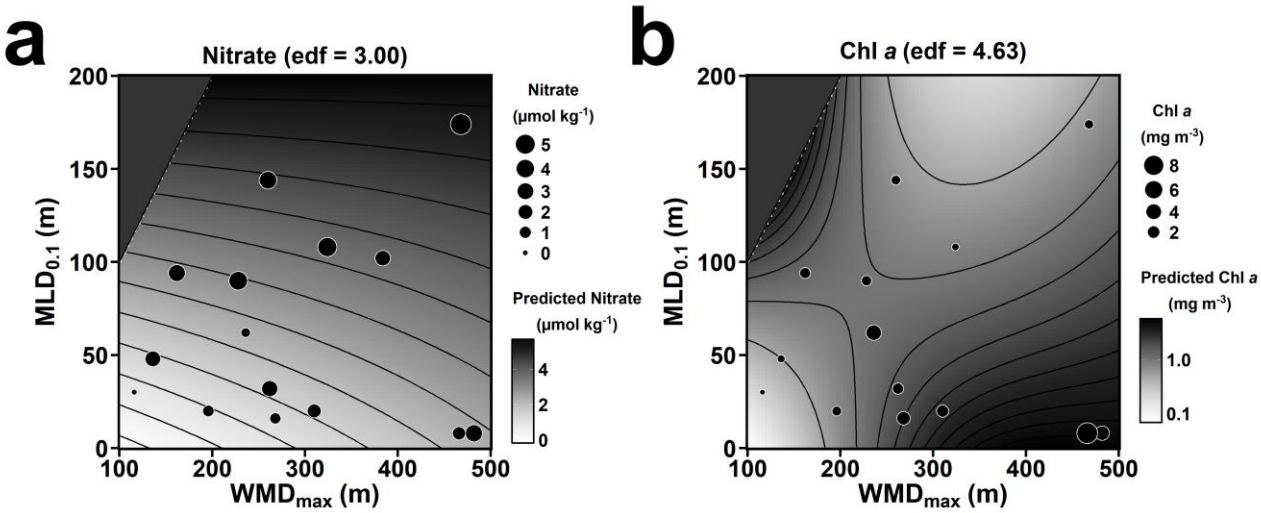


**Fig. 7 (b/w).** Observed (dot size) and predicted (contour plot) concentrations of **(a)** nitrate and **(b)** Chl *a* at surface (~ 0 m depth) in March. Predicted values were obtained based on the generalized additive model (GAM) in Table 2 that included an interaction term between the maximum winter mixing depth ($WMD_{max}$) and the near-surface stratification depth ($MLD_{0.1}$) in March. This interaction term had a p-value < 0.010 or < 0.050 for nitrate and Chl *a* concentration, respectively. The estimated degrees of freedom (edf) for each model are indicated. The dark gray triangles on the top left corners delimit those combinations of $WMD_{max}$ and $MLD_{0.1}$ that are not possible ($WMD_{max}$ cannot be shallower than $MLD_{0.1}$). Note that predicted Chl *a* concentrations are shown in $log_{10}$ scale.

904

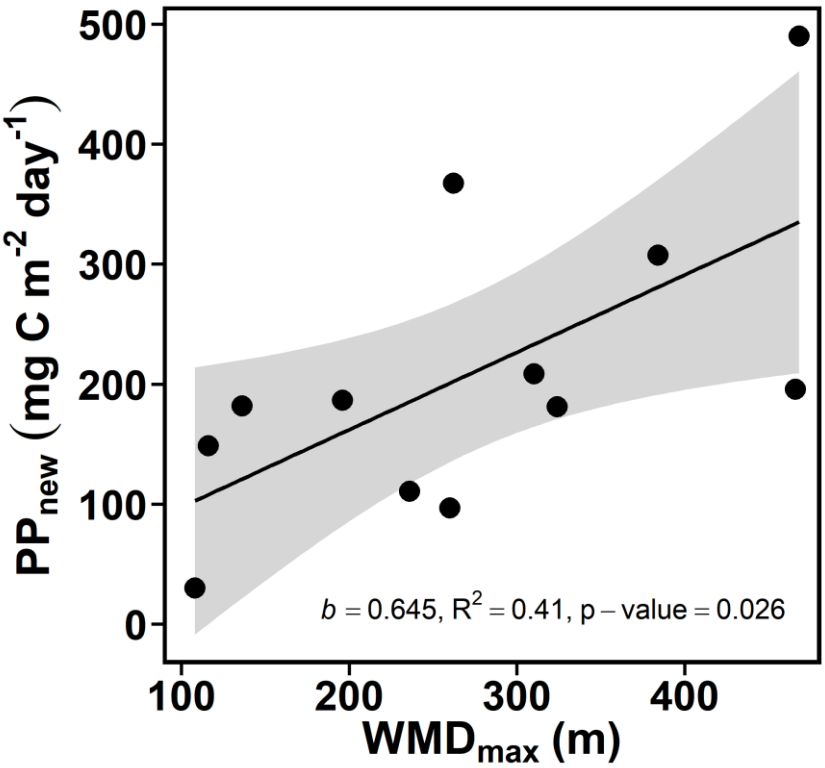


**Fig. 8.** Linear relationship between the new primary production ($PP_{new}$) in the upper 50 m of the water column between February and April and the maximum winter mixing depth ($WMD_{max}$). The shaded area represents the 95% confidence interval associated with the linear correlation. The slope (*b*), proportion of variance explained ($R^2$) and p-value of the relationship are shown.

905

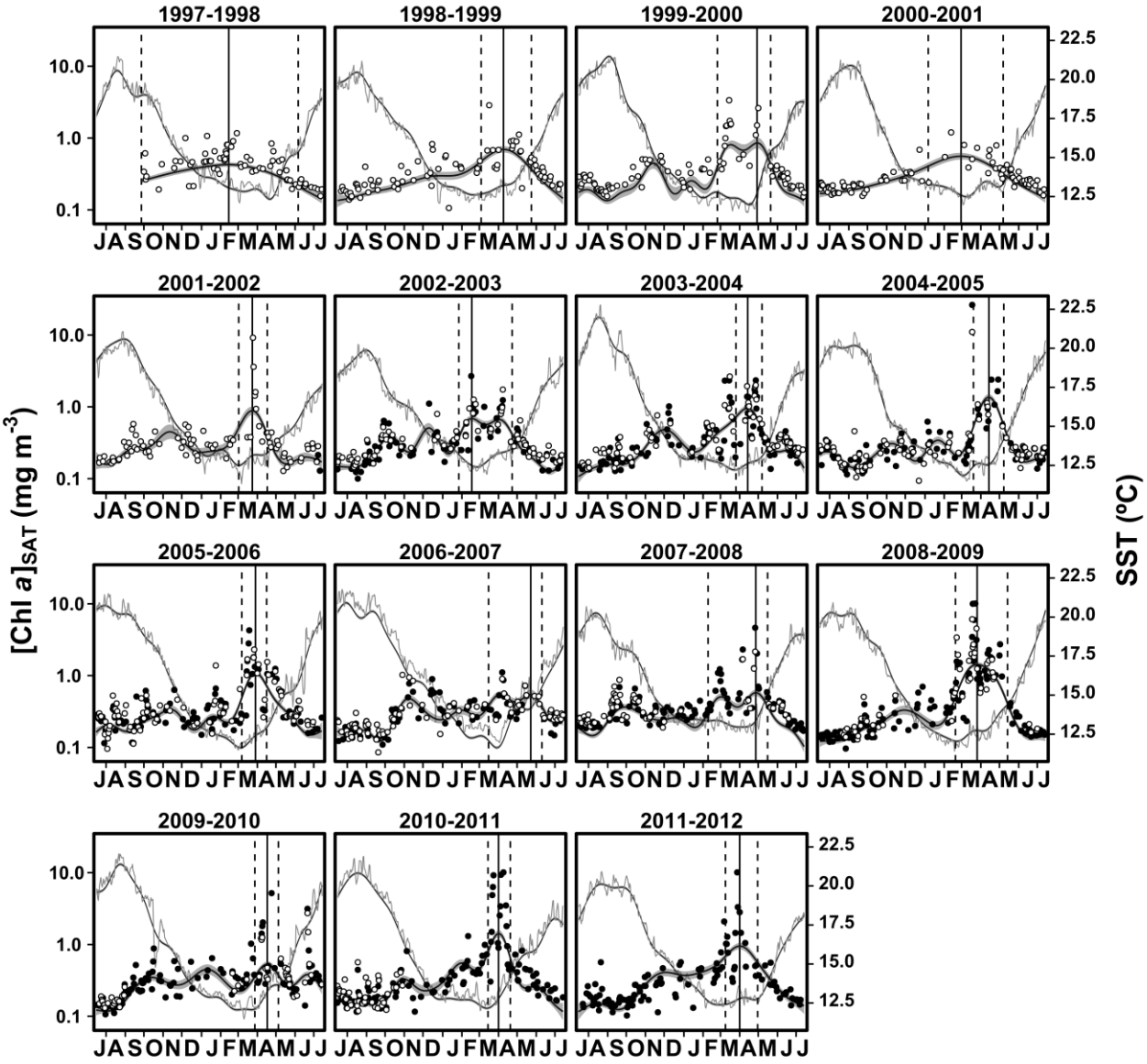


**Fig. 9** Sea surface temperatures (SST, light gray line) and Chl *a* concentrations ([Chl *a*]$_{SAT,}$ dots) from 1997 to 2012 based on satellite retrievals. Dot color indicates the sensor used to get the [Chl a]$_{SAT}$ measurements (white for SeaWifs and black for Aqua MODIS). Estimated seasonal cycles for SST (dark gray line) and [Chl *a*]$_{SAT}$ (black line) and their associated 95% confidence intervals (shaded areas) are based on the generalized additive model (GAM) predictions. The estimated degrees of freedom (edf) of the model varied between 16.19 and 18.53 for SST or between 3.19 and 13.42 for [Chl *a*]$_{SAT}$. Vertical solid lines indicate the maximum estimated [Chl *a*]$_{SAT}$ during the spring bloom. The initiation and termination day of the spring bloom are marked with vertical dashed lines. Note that [Chl *a*]$_{SAT}$ is shown in $\log_{10}$ scale and that the beginning of the seasonal cycle is set to July 15$^{th}$ (or 14$^{th}$ in a leap year).

906

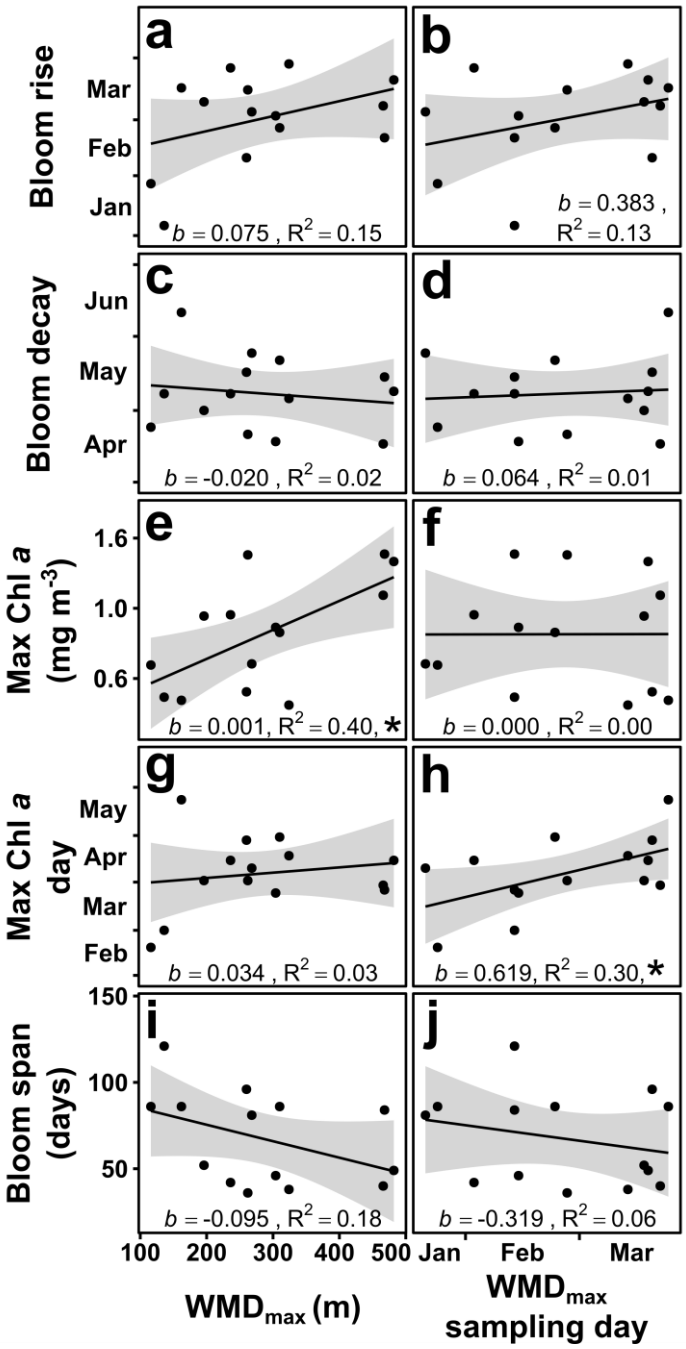


**Fig. 10.** Impact of the intensity and timing of the maximum winter mixing depth ($WMD_{max}$ and $WMD_{max}$ sampling date, respectively) on spring bloom metrics: **(a-b)** bloom rise, **(c-d)** bloom decay, **(e-f)** max Chl *a*, **(g-h)** max Chl *a* timing and **(i-j)** bloom span. The spring bloom metrics were derived from a generalized additive model (GAM) based on satellite data. The shaded areas associated with each linear relationship depict the 95% confidence intervals. The slope (*b*) and proportion of variance explained ($R^2$) of each relationship are shown. Those linear regressions with a p-value <0.050 are indicated with a *. Note that max Chl *a* is shown in $log_{10}$ scale.

907

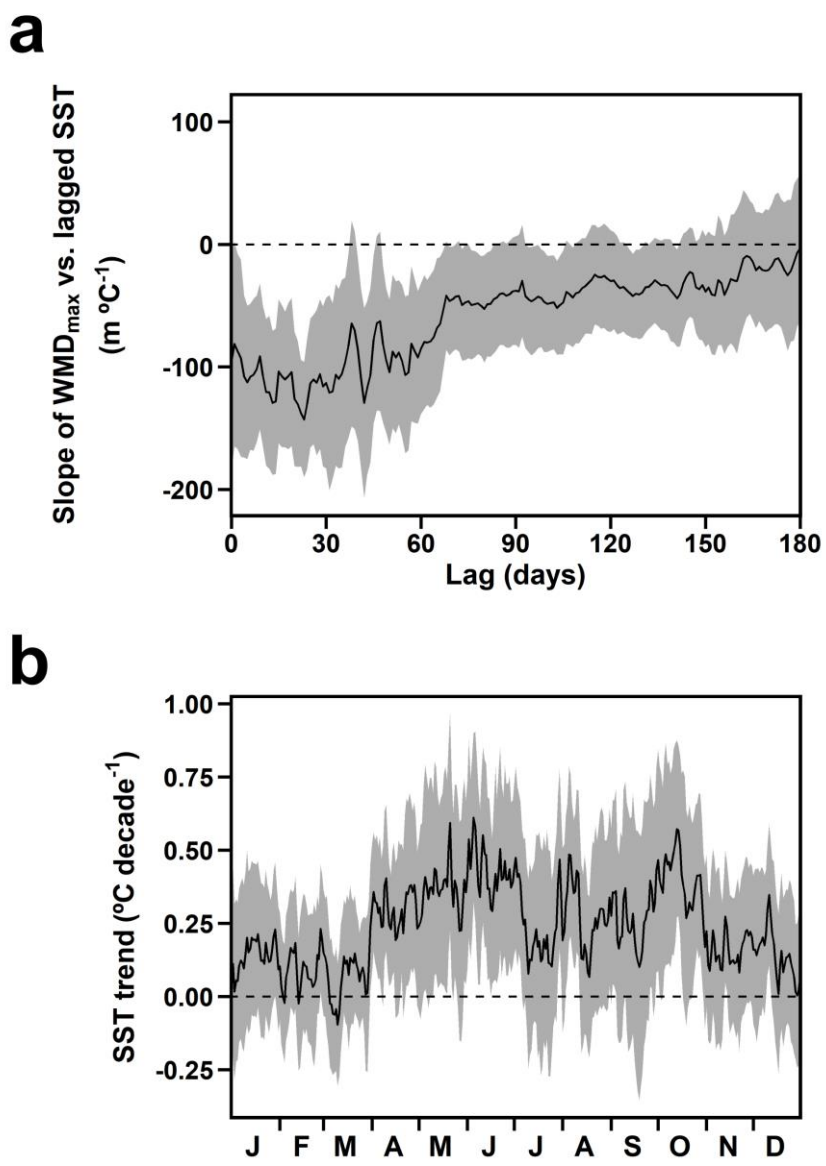


**Fig. 11. (a)** Variations in the slope of the linear relationships between maximum winter mixing depth ($WMD_{max}$) and the Sea Surface Temperature (SST) based on satellite retrievals at different day lags (1993-2012). **(b)** Long-term linear trends in SST (1981-2012) for each day of the year. Dashed horizontal lines indicate zero values. Shaded areas depict the 95% confidence intervals associated with the regression slopes.

908

## Tables

**Table 1.** Results from the model selection for the assessment of the effect of winter mixing depth ($WMD_{max}$) and our proxy for the thickness of the surface stratified layer ($MLD_{0.1}$) on nitrate and Chl *a* concentration at all depths (both represented as *y* in the formulas) in March. All models included an intercept ($a$) and an error term ($\varepsilon$). In addition, the generalized additive models (GAMs) incorporated through a smooth function ($f$, see *Supporting information* for further details) the influence of depth ($z$), or also the effect of the interaction ($te$) between $MLD_{0.1}$ or $WMD_{max}$ and depth. We report for each model the Akaike Information Criterion (AIC) and its associated weight (Burnham and Anderson 2002), and the proportion of variance explained ($R^2$). In all cases, the overall model had a p-value < 0.001.

| | | Nitrate | | | Chl *a* | | |
|---|---|---|---|---|---|---|---|
| **Model** | **What does the model estimate?** | **AIC** | **AIC weight** | **$R^2$** | **AIC** | **AIC weight** | **$R^2$** |
| $y = a + \varepsilon$ | Null model (includes only an intercept). | 598.80 | 0.00 | 0.00 | 222.61 | 0.00 | 0.00 |
| $y = a + f(z) + \varepsilon$ | Effect of depth. | 534.20 | 0.00 | 0.36 | 139.50 | 0.00 | 0.47 |
| $y = a + f(z) + te(WMD_{max}, z) + \varepsilon$ | Effect of winter mixing through the water column while accounting for the influence of depth. | 452.09 | 0.00 | 0.64 | 122.99 | 0.00 | 0.56 |
| $y = a + f(z) + te(MLD_{0.1}, z) + \varepsilon$ | Effect of stratification through the water column while accounting for the influence of depth. | 513.04 | 0.00 | 0.48 | 131.77 | 0.00 | 0.54 |
| $y = a + f(z) + te(MLD_{0.1}, z) + te(WMD_{max}, z) + \varepsilon$ | Combined effect of stratification and winter mixing through the water column while accounting for the influence of depth. | 419.50 | 1.00 | 0.73 | 101.29 | 1.00 | 0.65 |

**Table 2.** Results from the model selection for the assessment of the effect of winter mixing depth ($WMD_{max}$) and our proxy for the thickness of the surface stratified layer ($MLD_{0.1}$) on nitrate and Chl *a* concentration (both represented as *y* in the formulas) at the surface (~ 0 m depth) in March. All models included an intercept ($a$) and an error term ($\varepsilon$). In addition, the generalized additive models (GAMs) incorporated a smooth function ($f$ see *Supporting information* for further details) to estimate the effect of $WMD_{max}$, $MLD_{0.1}$ or their interaction ($te$, last model). We report for each model the Akaike Information Criterion (AIC) and its associated weight (Burnham and Anderson 2002), and the proportion of variance explained ($R^2$). The p-values for the overall model are also shown.

| | | Nitrate | | | | Chl *a* | | | |
|---|---|---|---|---|---|---|---|---|---|
| **Model** | **What does the model estimate?** | **AIC** | **AIC weight** | **$R^2$** | **p-value** | **AIC** | **AIC weight** | **$R^2$** | **p-value** |
| $y = a + \varepsilon$ | Null model (includes only an intercept). | 60.63 | 0.00 | 0.00 | 0.000 | 20.12 | 0.00 | 0.00 | 0.572 |
| $y = a + f(WMD_{max}) + \varepsilon$ | Effect of winter mixing. | 59.92 | 0.00 | 0.17 | 0.132 | 17.42 | 0.02 | 0.29 | 0.049 |
| $y = a + (MLD_{0.1}) + \varepsilon$ | Effect of stratification. | 51.51 | 0.21 | 0.52 | 0.002 | 19.78 | 0.01 | 0.15 | 0.165 |
| $y = a + f(MLD_{0.1}) + f(WMD_{max}) + \varepsilon$ | Independent combined effect of stratification and winter mixing. | 49.70 | 0.53 | 0.63 | 0.003 | 15.14 | 0.06 | 0.48 | 0.030 |
| $y = a + te(WMD_{max}, MLD_{0.1}) + \varepsilon$ | Interactive combined effect of winter mixing and stratification. | 51.16 | 0.26 | 0.64 | 0.008 | 9.72 | 0.91 | 0.75 | 0.016 |